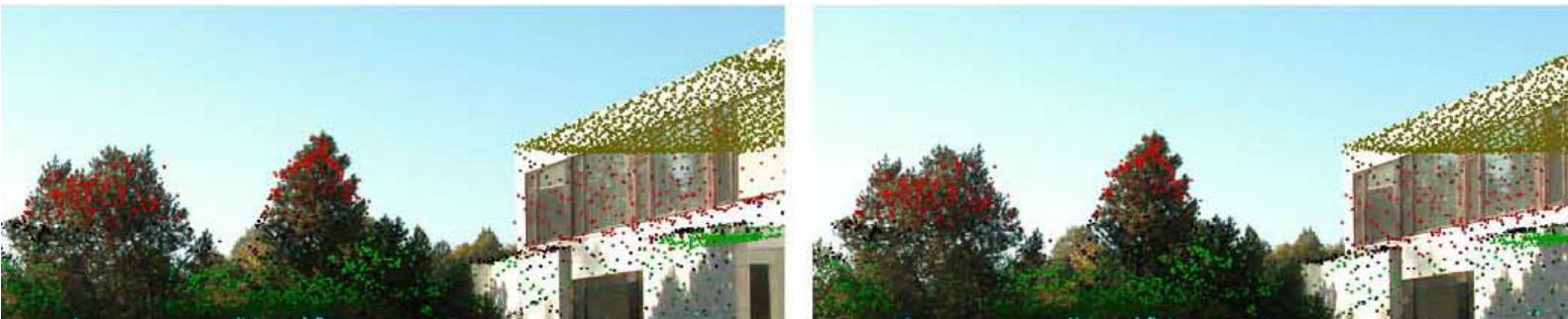# ORIENTATION AND INTEGRATION OF IMAGES AND IMAGE BLOCKS WITH LASER SCANNING DATA

Doctoral Dissertation

Petri Rönnholm

Aalto University

School of Science and Technology

Faculty of Engineering and Architecture

Department of Surveying

ORIENTATION AND INTEGRATION OF IMAGES AND IMAGE BLOCKS WITH LASER SCANNING DATA

Petri Rönnholm

Dissertation for the degree of Doctor of Science in Technology to be presented with due permission of the Department of Surveying, Aalto University School of Science and Technology for public examination and debate in auditorium M1 at Aalto University (Espoo, Finland) on the 12th of November, 2010 at 12 o´clock noon.

Abstract

Laser scanning and photogrammetry are methods for effective and accurate measurement and classification of urban and forest areas. Because these methods complement each other, then integration or integrated use brings additional benefits to real-life applications. However, finding tie features between data sets is a challenging task since laser scanning and imagery are far from each other in nature.

The aim of this thesis was to create methods for solving relative orientations between laser scanning data and imagery that would assist in near-future applications integrating laser scanning and photogrammetry. Moreover, a further goal was to create methods enabling the use of data acquired from very different perspectives, such as terrestrial and airborne data. To meet these aims, an interactive orientation method enabling the use of single images, stereo images or larger image blocks was developed and tested. The multi-view approach usually has a significant advantage over the use of a single image.

After accurate orientation of laser scanning data and imagery, versatile applications become available. Such applications include, e.g., automatic object recognition, accurate classification of individual trees, point cloud densification, automatic classification of land use, system calibration, and generation of photorealistic 3D models. Besides the orientation part, another aim of the research was to investigate how to fuse or use these two data types together in applications. As a result, examples that evaluated the behavior of laser point clouds in both urban and forestry areas, detection and visualization of temporal changes, enhanced data understanding, stereo visualization, multi-source and multi-angle data fusion, point cloud colorizing, and detailed examination of full waveform laser scanning data were given.

I

II

Tiivistelmä

Laserkeilaus ja fotogrammetriset menetelmät soveltuvat rakennetun ja rakentamattomien alueiden kolmiulotteiseen tiedon mittaamiseen sekä kohteiden luokittelemiseen. Laserkeilaus ja fotogrammetria täydentävät toisiaan, minkä johdosta aineistojen integrointi tai yhteiskäyttö on mielekästä. Koska menetelmät tuottavat luonteeltaan erilaista aineistoa, sopivien vastinpiirteiden löytyminen on usein haasteellista.

Tutkimuksen tavoitteena oli ratkaista laserkeilaus- ja kuva-aineistojen välisiä keskinäisiä orientointeja. Lisäksi haluttiin kehitettävien menetelmien mahdollistavan orientoinnit eri perspektiiveistä, kuten maasta ja ilmasta, otetuille aineistoille. Ongelman ratkaisemiseksi kehitettiin ja testattiin interaktiivista orientointimenetelmää, joka soveltuu käytettäväksi yksittäisten kuvien, stereokuvien sekä laajempien kuvajoukkojen kanssa. Tulosten mukaan eri perspektiiveistä otetuista kuvista muodostuvan kuvajoukon käyttö on usein mielekkäämpää kuin yksittäisen kuvan käyttö.

Useat sovellukset ovat mahdollisia vasta, kun laserkeilausaineistot ja kuvat ovat orientoituna samaan koordinaatistoon. Sovellusesimerkkeinä voidaan mainita esimerkiksi automaattinen kohteiden tunnistaminen, yksittäisten puiden mallintaminen, pistepilvien tihentäminen, automaattinen maankäytön luokittelu, järjestelmien kalibrointi sekä fotorealististen 3D mallien tuottaminen. Orientointien ratkaisemisen lisäksi työn tavoitteena oli myös tutkia aineistojen fuusiota sekä yhteiskäyttöä. Tuloksena esitettiin esimerkkejä laserkeilausaineistojen käyttäytymisestä rakennetussa ja rakentamattomassa ympäristössä, havaittiin ja visualisoitiin ajasta johtuvia muutoksia, parannettiin datojen tulkittavuutta sekä visualisoitiin aineistoja stereona. Lisäksi fuusioitiin eri lähteistä ja eri perspektiiveistä otettuja aineistoja, värjättiin pistepilviä ja tutkittiin yksityiskohtaisesti täyden kaiun laserkeilausaineistoa.

IV

PREFACE

The research presented in this thesis was carried out at the Institute of Photogrammetry and Remote Sensing during 1999-2010 under the supervision of Professor Henrik Haggrén. I am most grateful to him for his encouragement, inspiration and support during this work. My sincere gratitude goes also to Doctor Hannu Hyyppä and Professor Juha Hyyppä, who have greatly supported my work.

I like to thank my current and former colleagues at the Institute of Photogrammetry and Remote Sensing. They have helped me in many ways by giving support, advice and assistance to my work as well as creating the inspiring working environment. Especially, I would like to thank Keijo Inkilä, who has given me valuable advice during my work. I also would like to thank many colleagues from the Finnish Geodetic Institute for fruitful co-operation.

I am very grateful to my pre-examiners, Professor Ayman Habib and Professor Norbert Pfeifer, for valuable comments and support on this thesis.

Finally, I would like to thank my parents, Nils and Seija, for all they have given me, my wife Taina for her love and support during this process, and our children Sauli and Heidi for the joy they have brought into my life.

Espoo, July 28, 2010
Petri Rönnholm

VI

Contents

List of Publications

This thesis is based on the following publications, referred to in the text by their Roman numerals:

I   Rönnholm, P., Honkavaara, E., Litkey, P., Hyyppä, H., and Hyyppä, J., 2007. Integration of laser scanning and photogrammetry (Key-note). *International Archives of Photogrammetry, Remote Sensing and Spatial Information Sciences*, 36(Part 3/W52), pp. 355-362.

II   Rönnholm, P., Hyyppä, H., Pöntinen, P., Haggrén H., and Hyyppä, J., 2003. A method for interactive orientation of digital images using backprojection of 3D Data. *The Photogrammetric Journal of Finland*, *18*(2):58-69.

III Rönnholm, P., Hyyppä, H., Hyyppä, J., and Haggrén, H., 2009. Orientation of airborne laser scanning point clouds with multi-view, multi-scale image blocks. *Sensors*, 9, pp. 6008-6027.

IV   Rönnholm, P., Hyyppä, J., Hyyppä, H., Haggrén, H., Yu, X. and Kaartinen, H., 2004. Calibration of laser-derived tree height estimates by means of photogrammetric techniques. *Scandinavian Journal of Forest Research*, *19*(6):524-528.

V   Litkey, P., Rönnholm, P., Lumme, J., and Liang, X., 2007. Waveform features for tree identification. *International Archives of Photogrammetry, Remote Sensing and Spatial Information Sciences*, 36(Part 3/W52), pp. 258-263.

VI   Hyyppä, H., Rönnholm, P., Soininen, A., and Hyyppä, J., 2005. Scope for laser scanning to provide road environment information. *The Photogrammetric Journal of Finland*, 19(2):19-33.

II, **III**, **IV**, and **VI** are PEER reviewed journal articles; **I** and **V** are PEER reviewed conference articles.

x

Author's contribution

In paper **I**, I described the general strategies for solving the orientation between laser scanning data and images. I also discuss the error sources that may reduce the accuracy of the orientation. I have written most of the text and I am responsible for almost all the images that illustrate the integration of laser scanning data and images. The levels of integration that were presented in Chapter 3 were created in co-operation with Eija Honkavaara. In addition, Eija assisted me in associating false-colors from aerial images with the laser point cloud in Figure 8. Hannu Hyyppä assisted me with Figures 2 and 7 and also arranged airborne laser scanning data sets. Paula Litkey assisted me in handling full waveform data. Juha Hyyppä was an adviser.

In paper **II**, I developed a novel method for solving the relative orientation between laser scanning data and a single image. I was responsible for all text, software development, methods and accuracy testing. Petteri Pöntinen assisted me with image acquisition and the creation of panoramic images. Hannu Hyyppä and Juha Hyyppä were advisers. Henrik Haggrén was the supervisor.

In paper **III**, I extended the original method, presented in paper **II** to be suitable for orientation between laser scanning data and image blocks. I developed the concept and was responsible for software development, testing and for writing the article. Hannu Hyyppä and Juha Hyyppä were advisers. Henrik Haggrén was the supervisor.

In paper **IV**, I applied a developed interactive orientation method in order to explain why laser scanning data usually underestimates tree height. I was responsible for planning and completing the experiment and comparisons, and for writing the major sections of the text. Juha Hyyppä assisted with writing. Harri Kaartinen was responsible with collecting the reference heights of trees with the total station. Hannu Hyyppä, Juha Hyyppä and Xiaowei Yu were advisers. Henrik Haggrén was the supervisor.

In paper **V**, I planned and completed orientation of full waveform laser data and images, and I was responsible for developing software for demonstrating orientation, and the integrated use of data. My experiments were presented in Chapter 3.3., which I also wrote. Xinlian Liang was responsible for Chapter 3.1.1., Paula Litkey for Chapter 3.1.2, and Juho Lumme for Chapters 3.2.1 and 3.2.2.

In paper **VI**, I contributed as co-author. I was responsible for registering images and laser scanning data as well as assisting with data analysis. Hannu Hyyppä was the author responsible for writing the paper.

List of Abbreviations

2D	Two dimensional
3D	Three dimensional
AMCW	Amplitude Modulated Continuous Wave
CCD	Charge Coupled Device
CIR	Color Infrared
DEM	Digital Elevation Model
DGPS	Differential Global Positioning System
DSM	Digital Surface Model
DTM	Digital Terrain Model
EuroSDR	European Spatial Data Research
e.g.	exempli gratia
etc.	et cetera
FMCW	Frequency Modulated Continuous Wave
FOV	Field Of View
GPS	Global Positioning System
i.e.	id est
ICP	Iterative Closest Point
in situ	Latin phrase meaning in the place
IfSAR	Interferometric SAR
IMU	Inertial Measurement Unit
LIDAR	LIght Detection And Ranging
nDSM	Normalized Digital Surface
NDVI	Normalized Difference Vegetation Index
NIR	Near Infrared
Radar	RAdio Detection And Ranging
RANSAC	Random Sample Consensus
RGB	Red Green Blue (image color channels)
RTK	Real-Time Kinematic
SAR	Synthetic Aperture Radar
TOF	Time-of-Flight
UAV	Unmanned Aerial Vehicle

List of Symbols

c	principle distance
X_0, Y_0, Z_0	projection center of a camera
X, Y, Z	3D point in the ground coordinate system
x, y	3D point in the image coordinate system
x_0, y_0	location of a principle point in the image coordinate system
$r_{11}...r_{33}$	elements of a 3D rotation matrix
Δr	amount of radial lens distortion
r	distance from the distortion centre of an image
K_1, K_2, K_3	three first coefficients for correcting radial lens distortion
P_1, P_2, P_3	three first coefficients for correcting decentering lens distortion
$\Delta x_{radial}, \Delta y_{radial}$	amount of corrections of radial lens distortions
c_x, c_y	distortion centre of an image
x_c, y_c	image point, when the origin is shifted to the distortion centre of an image
$\Delta x_{decentric}, \Delta y_{decentric}$	amount of corrections of decentering lens distortions
$x_{corrected}, y_{corrected}$	image point after radial and decentering lens distortions
ω, φ, κ	rotation angles around the axes of a camera coordinate system
α, ν, κ	rotation angles: azimuth, tilt, swing
$R, R1, R2$	3D rotation matrices
n	amount of shift in the ground coordinate system units
O	origin
U	relative 3D rotation matrix between two coordinate systems
b	camera base, i.e. distance between two projection centers
$P1_0, P2_0, P_{0\_after}$	projection centers of cameras
$\Delta X, \Delta Y, \Delta Z$	3D coordinate differences
$\Delta\omega, \Delta\varphi, \Delta\kappa$	rotation differences

List of Figures

XVI

List of Tables

1 Introduction

> *The instant the atmosphere is illuminated it will be filled with an infinite number of images which are produced by the various bodies and colors assembled in it. And the eye is the target, a lodestone, of these images.*
>
> *--Leonardo da Vinci*

1.1 Background

Accurate mapping of our environment has had and will have an important role in societies. Mapping of large areas requires proper instruments and methods. The most important methods for data acquisition are geodetic measurements, photogrammetric methods, laser scanning, radar and sonar (Figure 1). This thesis focuses on laser scanning and photogrammetric methods.

Both terrestrial and aerial laser scanning have had an enormous impact on the development of 3D data acquisition. However, quite soon, researchers and system developers realized that that the laser point clouds alone were not necessarily providing as much information as was desired. In particular, classification and identification of objects using laser scanning data can be very difficult if no additional optical sensors are available (Baltsavias, 1999). As early as the 1980s, when airborne laser scanning was merely a profile measurement technique, laser points were used together with aerial images (Aldred and Bonnor, 1985). Even although modern airborne laser scanners provide relatively dense 3D point clouds, they provide only irregularly distributed object points (Habib et al., 2005). Therefore, laser scanning does not directly capture breaklines as well as the photogrammetric imagery (Mitishita et al., 2008).

Photogrammetric images[1] provide much complementary information for laser scanning (Kern, 2001; Schenk and Csathó, 2002) – and vice versa. The availability of several color bands combined with well known internal geometry and the possibility of making 3D measurements from images makes photogrammetry the most relevant method used with laser scanning data. Despite the fact that photogrammetric methods have been

---

[1] Images can be captured using many devices and not, only with optical cameras. In this context, however, photogrammetric measurements are carried out using photographic images or imagery.

available for almost 200 years (Konecny, 1985), they have developed rapidly during the last decades. The first fully digital camera system, the Fujix DS-1P, was released in 1988 (Tarrant, 2007). The first digital large-format aerial camera systems, the Z/I Imaging DMC and the Leica ADS40, were introduced in 2000. Today, digital cameras have almost completely replaced film cameras in modern photogrammetric processes. At the same time, photogrammetric software (e.g. Fraser and Hanley, 2004; Menci and Rinaudo, 2007; Lemmens, 2007b) has become more productive and flexible than previously.

The integrated use of laser scanning data and digital images allows the automated creation of 3D models that are more accurate and of better quality. In addition, integration of images and laser scanning data is an excellent combination for obtaining rigorous quality control of laser scanning data (Schenk and Csathó, 2002). The main concern when integrating data from multiple data sources is, however, that all the data are oriented into the same coordinate system. Because the nature of these data sources is different, the orientation is not trivial. Therefore, there are also future scenarios relying only on hyperspectral laser scanning (Kaasalainen et al., 2007). The advantage of the hyperspectral laser is that it also provides, in addition to the geometry, the hyperspectral response of the target measured, which improves, e.g., automatic classification of objects.

	Geodetic measurements	*Data acquisition orientation integration*	Photogrammetry
Radar			-Aerial, terrestrial, satellite
Sonar	Laser scanning -hyperspectral		-RGB -CIR -multispectral -hyperspectral
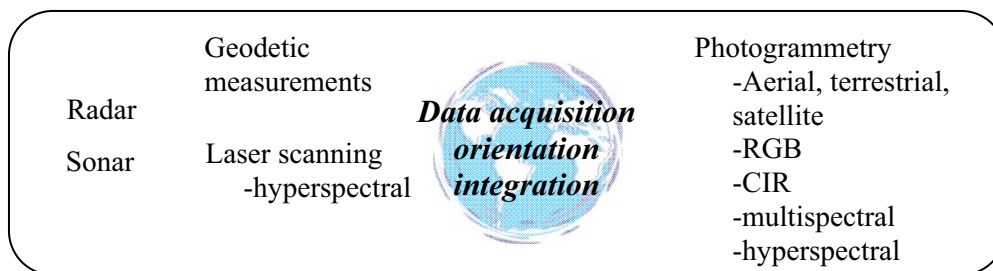
Figure 1. The most important methods for data acquisition. Data from any data acquisition method can be integrated with other information if relative orientation is well enough established.

Many examples of registration and integration of data from the same perspective, i.e. airborne laser scanning data with aerial images or terrestrial laser scanning data with terrestrial images, do exist. However, the potential of integrating data taken from different perspectives have been mostly neglected. The advantage of using different perspectives is that, typically, the differences in laser point clouds and image contents are more clearly visible. In addition, if a complete 3D model of our environment is required, both terrestrial and airborne data is needed (Böhm and Haala, 2005).

After a proper orientation phase, numerous amounts of applications, based on multi-source data, are available. Currently, the most promising end applications are, e.g., automatic object recognition, accurate classification of individual trees, point cloud densification, automatic classification of land use, system calibration, and generation of

photorealistic 3D models. However, it is quite obvious that the full potential of the integrated use of laser scanning data and images has not yet been applied. One obstacle that prevents integrated use may be orientation difficulties.

1.2   Objectives

The objective of the study was to develop methods for solving orientations between laser scanning data and digital images or image blocks without limitations from data acquisition perspective. The accuracies of orientations were examined. The hypothesis was that by adding more images taken from different perspectives, the accuracy of orientations would increase. In addition, using data from different perspectives was expected to provide more complete understanding of objects or areas of interest.

Since, prior to this research, terrestrial images had not been used with airborne laser scanning data, one sub-goal was to investigate how different viewing perspectives of data sources reveal the behavior of laser scanning data. Another sub-goal was to experience data fusion by colorizing laser point clouds from images that were acquired from very different perspectives, such as terrestrial and airborne images. In Figure 2, objectives are included in a flow chart of the complete process.
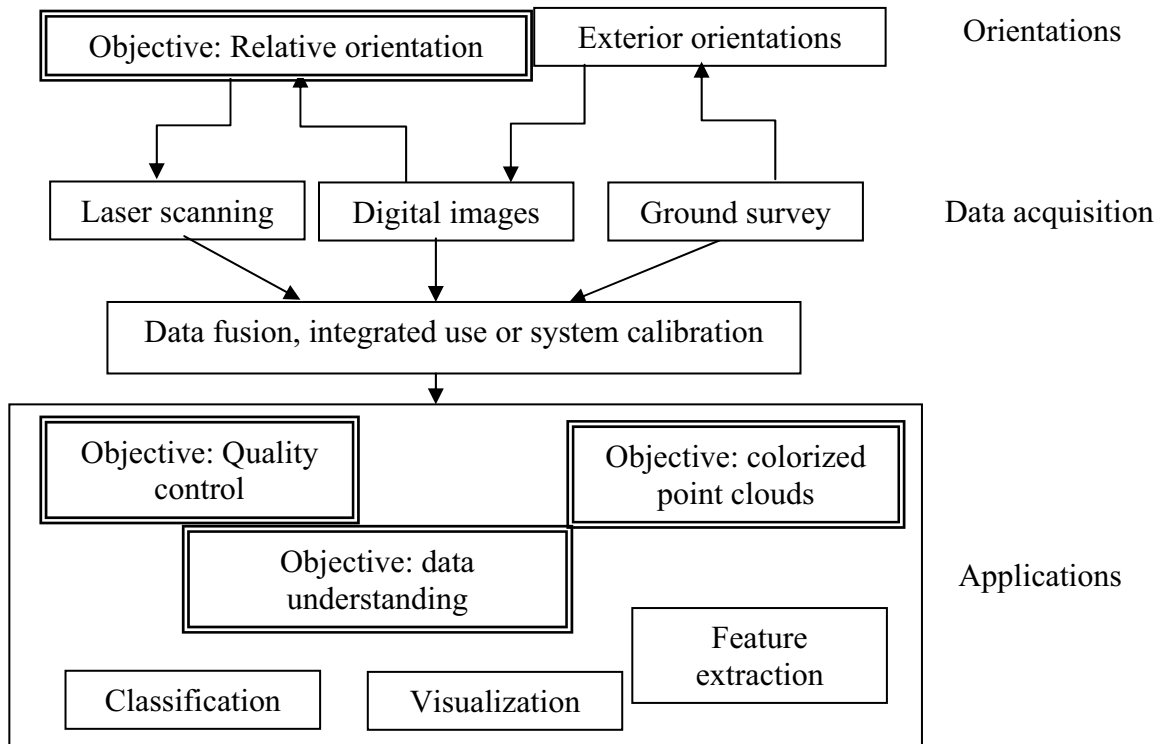
Figure 2. A workflow from data acquisition to applications. This workflow assumes that internal geometry of images and laser scanning has been calibrated and corrected.

1.3   Outline of the thesis

The thesis is organized as follows.

First, the motivation and background for the study are presented in Chapter 1. In addition, the objectives of the research are highlighted.

In Chapter 2, laser scanning and photogrammetry as technologies are introduced as well as the state-of-the-art of how to obtain multi-source data sets into the same coordinate system. In addition, the state-of-the-art regarding the integrated use of laser scanning data and images is presented.

Materials and methods of the research are described in Chapter 3. Here, the developed techniques are also presented.

In Chapter 4, the main results, reported originally in Publications **I-VI**, are summarized.

The discussion about the applicability of the developed method, a comparison with other research and information on future research are included in Chapter 5.

The results and the main conclusions of the thesis are summarized in Chapter 6.

2 Review

2.1 Core technologies

In following two chapters, the main data acquisition technologies, laser scanning and photogrammetry, are briefly introduced. Both data acquisition methods are typically supported with geodetic reference measurements, such as static GPS, RTK GPS or total station measurements, in order to achieve accurate transformation into the ground coordinate system.

2.1.1 Laser scanning

Laser scanning is based on LIDAR distance measurements and the known location and attitude of a sensor. There exist several different implementations on devices and platforms, in which the scanners can be mounted. The mount can be a satellite, an aircraft, a helicopter, an unmanned aerial vehicle (UAV) (Jaakkola et al., 2010), a vehicle, a tripod, or a hand-held device, thus covering the laser scanning sub-disciplines: i.e. airborne laser scanning, UAV- and vehicle-based laser scanning, terrestrial laser scanning and hand-held laser scanning. The distance measurement can be made by using time-of-flight (TOF) or by triangulation (Blais, 2004). Because, typically, systems based on triangulation are utilized only for relatively short-range measurement, they are not commercially available for space- or airborne solutions. However, Haggrén et al. (1995) report an experiment, in which a triangulation-based airborne laser system was utilized for modeling ice fields. Furthermore, TOF systems can function using three different methods. The first method utilizes pulse ranging, in which the traveling time of a single light pulse is measured directly. The second method uses amplitude modulated continuous wave (AMCW), called also as phase-shift ranging. In this method, the traveling time of the light is derived from the phase shift of the transmitted and the received modulated signal. Jarvis (1983) highlights the early development of pulse ranging and phase-shift systems. The third method uses frequency modulated continuous wave (FMCW) (Hulme et al., 1981), in which the traveling time of the light is derived from the systematic variation of the frequency of a modulated signal. A more detailed discussion about the advantages and disadvantages of pulse ranging and continuous wave technologies is presented by Wehr and Lohr (1999).

Typically, the AMCW and FMCW systems are used in mid-range terrestrial or mobile devices having the advantage of fast data acquisition. However, pulse systems are more

accurate at long ranges. Therefore, for example, most airborne laser scanners use the pulse ranging technique (Pfeifer and Briese, 2007). Conventional airborne laser scanners can only have one light pulse in the air at one time limiting the data acquisition speed. However, recently new devices have been developed that can have multiple pulses in the air simultaneously.

Frame-based ranging devices, named as range imaging cameras or laser range cameras, are able to capture practically simultaneously a complete scene in 3D (e.g. Schroeder et al., 1999; Lange and Seitz, 2000; Oggier et al., 2004). The potential of such instruments is high. Currently, the resolution and accuracy of range images limits their use in less accurate modeling tasks. However, their ability for real-time 3D modeling enables several applications, such as automatic vehicle guidance, face detection, monitoring of moving objects in 3D, 3D gaming, and automatic detection of pedestrians in order to avoid collision, to name just a few. The performance of range cameras can be improved by calibration (Kahlmann and Ingensand, 2005; Lichti, 2008).

The wavelength of the laser beam plays a key role in how the light interacts with objects. The majority of airborne laser scanners use near infrared wavelengths, such as 900 nm or 1064 nm, or middle infrared, such as 1550 nm. Lemmens (2007a), for example, gives a list of airborne laser scanning systems and their wavelengths. However, the preferred wavelength for bathymetric laser scanners is 532 nm, because green light penetrates the water surface (LaRocque and West, 1999). Therefore, underwater measurements are also available – with some limitations. In the case of clear water, the penetration of a 532 nm laser beam is quite deep, but any particles in the water disturb the measurements, which limits the measuring depth. In the case of terrestrial laser scanners, there is much variation in the applied wavelength, and in some devices the wavelength is even adjustable. The wavelengths of many terrestrial laser scanners can be found, e.g., in Lemmens (2009).

One advantage of laser scanners is that a single light beam can hit multiple targets before completely returning to the device. The cause of this phenomenon is that the laser beam broadens according to the divergence angle. In the case of vegetation or breaklines, usually, some parts of a light beam penetrate behind the first objects and give information about the objects behind the first one. Therefore, one range measurement in full waveform data actually includes several range values and their intensities. Visualizations of full waveform laser scanning data can be found, e.g., in Persson et al. (2005) and in Paper **V**. Most laser scanners provide more than one echo return and some can record the full waveform. In addition to providing valuable information under the canopies, full waveform information has a large potential for, e.g., segmentation and classification purposes (Wagner et al., 2006; Wagner et al., 2008).

Airborne laser scanning systems rely on GPS and IMU systems, which are used to record the location and attitude of a laser sensor during the data acquisition. The use of these devices requires accurate system calibration, in which e.g. the relative locations and attitudes of each sensor are solved (Honkavaara et al., 2003). The accuracies of

airborne GPS/IMU systems are reported to be as high as 5–10 cm in position and better than 0.006º for ω and φ, and 0.01º for κ in rotations (Kremer, 2001; Heipke et al., 2002; Honkavaara et al., 2003). However, because the GPS and IMU systems has no inherit quality control (Schenk and Csathó, 2002), typically, some systematic or random deformations exist within a single airborne laser scanning strip. The usual method for overcoming this drawback is to allow adjacent laser strips to overlap and also to have cross strips in order to ensure successful strip adjustment. In addition to GPS/IMU errors, airborne laser scanners also suffer from many other error sources. Detailed description of these error sources can be found in Schenk (2001). According to Pfeifer (2005), two main approaches for correcting the internal errors of airborne laser scanning strips after data acquisition are data-driven methods (e.g. Kilian et al., 1996; Crombaghs et al., 2000; Kraus and Pfeifer, 2001; Vosselman and Maas, 2001; Kornus and Ruiz, 2003) and sensor-based methods (e.g. Burman, 2002; Filin, 2003; Kager, 2004). The advantage of sensor-based methods is that the corrections are physically connected to original GPS/IMU observations.

Additionally, vehicle-based laser scanning requires continuous positioning (e.g. El-Sheimy, 2005; Kukko et al., 2007). Direct orientation systems suffer from urban canyons and multiple reflectances, which cause errors in data. Therefore, post-processing is essential in order to achieve geometrically consistent point clouds.

More traditional terrestrial laser scanning acquires a single scan from a stable scanner location. Without dependence on the accuracy of GPS/IMU systems, typically such terrestrial devices are more accurate than mobile ones. However, these systems may also have problems in internal geometry. Typically, triangulation-based systems are more accurate than TOF-based laser scanners, if the measurement range does not exceed 10 meters (Blais et al., 2003). Lichti and Licht (2006) gave a detailed description about calibration and correction of various error sources of TOF laser scanners, such as rangefinder error, collimation axis error, trunnion axis error, non-orthogonality of the plane containing the horizontal angle encoder and vertical axis, horizontal direction encoder scale error, vertical circle index error, vertical eccentricity error and several types of sinusoidal errors that have either a physical explanation or can be empirically detected.

Laser scanners record the intensity value of laser echoes. Many factors affect to intensity values and therefore it is essential to calibrate them before use (Luzum et al., 2004). Kaasalainen et al. (2009) illustrates how commercially available or *in situ* reference targets can be used during a scanning campaign for the calibration of intensity values. Color values may be attached to a laser scanning point cloud, if a camera is integrated in the system or if an external image is oriented in the same coordinate system with laser data.

The workflow typical of airborne laser scanning is data acquisition, noise removal, data classification, data filtering, strip-wise adjustment of adjacent laser scanning strips, and orientation to the ground control. After these steps, data is processed for further applications. The applications typical of laser scanning are, e.g., forest inventory,

creation of digital elevation models and construction of virtual 3D city models. Rottensteiner et al. (2007) gives a detailed overview and comparison of current methods for extracting buildings from laser scanning data. For more detailed information on algorithms and airborne laser scanning methods that are commonly used for forest measurements, recent papers by Hyyppä et al. (2004; 2008) are recommended.

From Lemmens (2007) it can be seen that the precision of most commonly used airborne laser scanners vary between 0.04 and 0.15 meters in heights and 0.10 and 0.30 meters horizontally. This precision does not usually include systematic GPS errors. Ahokas et al. (2003) compared airborne laser scanning data with total station measurements in several test fields, recording differences in heights between 0.02 and 0.4 meters. Schenk et al. (2001) reported horizontal shifts of less than 0.40 meters when airborne laser scanning data was compared with photogrammetric measurements. In the case of TOF-based terrestrial laser scanners, range accuracies are typically between 0.002 and 0.02 meters and scan angle accuracy is between 0.0005° and 0.04° (Lemmens, 2009).

2.1.2   Photogrammetry

Photogrammetric measuring methods are widely used by, e.g., mapping sciences, industry, forestry, archeology, astronomy, the film industry, and robotics. Photogrammetric techniques rely on a known sensor and imaging geometry. A sensor model depends on the camera and lens type. The central perspective camera model is the most typical. To ensure that a real image meets an ideal model, the possible errors should be modeled and corrected. The lens system causes most of the errors. Therefore, the amount of lens distortions is solved during camera calibration. More details can be found in Chapter 3.2.

A single image represents a 2D perspective image of the scene. If two or more images are available, the 3D scene can be reconstructed using forward intersections of light rays observed in images. The photogrammetric techniques have been available since the 19th century, but they are still being developed enthusiastically. Digital cameras have replaced film cameras thus enabling more efficient photogrammetric processes, because film development and scanning are no longer needed. In addition, the internal geometry of digital cameras is more stable when compared with that of film cameras. However, panchromatic images of modern digital large-format aerial cameras are typically image mosaics from several sub-images. Practical experiments about calibration of digital aerial cameras can be found in EuroSDR's publication by Cramer (2009).

A camera is able to capture the scene using a corresponding color palette with human vision. Therefore, images contain much semantic, as well as geometric, information and thus visual interpretation is intuitively easy. However, typical RGB color channels are not only possible selection for imaging. Some cameras are able to record also other areas of the spectral band. The most common alternatives for RGB images are infrared

bands, such as near- or thermal infrared bands. Some sensors are also able to detect gamma radiation in a scene. Combining different spectral bands, special images may be created that highlight different things than common RGB images. Typical examples of such special images are color infrared (CIR) images. CIR images can be used for distinguishing vegetation from built-up areas. In addition, other products, such as NDVI, can be calculated when a near-infrared channel (NIR) is available.

$$NDVI = \frac{NIR - RED}{NIR + RED} \qquad (1)$$

Stereo viewing of images assists greatly in manual interpretation and measurements. However, stereo and multi-images can be used for automatic or semiautomatic scene reconstruction. The stereo matching process can be divided roughly into two main approaches, which are area-based matching and feature-based matching. In addition, these two matching strategies can be combined into a hybrid method (e.g., Koschan, 1993; Liu et al., 2004; Silveira et al., 2008). Area-based methods select a small area from one image and try to find the best match from another image. The search area can be greatly reduced if the relative orientation between images is already known. Feature-based methods extract automatically features, such as corners, edges, lines, curves, circles, ellipses or regions, and search corresponding feature pairs. The main drawback of stereo matching is that in the case of textureless areas it fails. In addition, changes in perspective and illumination or a repeating pattern in the textures cause mismatches. The use of multi-image matching (e.g. Maas, 1996) increases reliability and precision because of improved imaging geometry. The disadvantage of multi-image methods is that the image overlap should be 60%-80%.

In the case of terrestrial imaging, the geometry of an image block can be designed more freely than in the aerial case. The imaging geometry can be optimized in order to achieve desired accuracy (Fraser, 1989). When close-range images are used, the narrow imaging angle may cause problems, leading to a need for a large set of images. In some cases, the use of panoramic imaging (Pöntinen, 2000; Luhmann, 2004), fish-eye lenses, or wide-angle lenses may be advisable. Typically, orientations of all images within an image block are solved in a bundle block adjustment (Triggs et al., 1999). The accuracy of photogrammetric measurements is highly dependent on imaging geometry, lenses, image resolution, distance to a target, type of a target, and image point measurement accuracy. However, even accuracies of 1:1000000 have been reported in the fields of close-range photogrammetry (Fraser, 1992).

2.2 Common coordinate system for images and laser scanning data

If images and laser scanning data are to be used together, they must be in the same coordinate system. Otherwise, an integrated data set may give misleading information

about areas that are not correctly overlapped. In principle, there exists three main strategies how to succeed with this:

1. System calibration of the hybrid device for simultaneous data acquisition
2. Separate orientation of images and laser scanning data to a common ground coordinate system
3. Relative orientation of images and laser scanning data

In addition, direct orientation sensors, GPS/IMU, provide a common coordinate frame. Unfortunately, as pointed out in Chapter 2.1.1, the accuracy of direct orientation sensors is usually not enough to enable imagery and laser scanning data to be integrated with a high degree of accuracy.

2.2.1 System calibration of the hybrid device for simultaneous data acquisition

System calibration of the hybrid device for simultaneous data acquisition requires that both a laser scanner and a camera are mounted on the same platform (e.g. Wendt and Dold, 2005; Przybilla, 2006). In this case, the relationship between instruments does not change, and once the system calibration has been performed, the acquired data can be transformed automatically into the same coordinate system. If the color information is collected co-axially aligned with the laser beam, color values can be applied directly to the laser point cloud (Ullrich et al., 2001). However, usually the camera is mounted externally to the laser scanner, in which case a system calibration is needed (Ullrich et al., 2003). Laser scanners that also have a camera attached or integrated are usually called hybrid laser scanners. Some examples on how hybrid laser scanners have been used in orientation or modeling processes are highlighted in Chapter 2.3.

Even if a system calibration has been utilized with terrestrial laser scanners, the acquisition of laser data and images typically is not simultaneous. Therefore, any changes that occur between the data acquisitions cause data sets to differ from each other. Actually, only frame-based ranging systems fulfill the demand of simultaneous data collection. Ray et al. (2001) illustrated several technological alternatives for how a color image can be integrated with a frame-based 3D range camera. If a scene contains only stable objects, a time-gap between data acquisitions is not important and a system calibration is valid for any stable hybrid laser scanners.

2.2.2 Separate orientation of images and laser scanning data

The second method relies on the separate orientation of both data sets into the common ground coordinate system. Typically, this requires measured ground control points or features. These ground control points or features are identified from images and laser

scanning data and parameters for transformations are solved. In many cases, unfortunately, the most suitable ground control features for laser scanning are not optimal for photogrammetric measurements, and vice versa. For terrestrial laser scanning, a great variety of artificial targets, differing with in shape and materials, have been suggested. The selection of materials is important since highly reflective materials may cause anomalies in range measurements and produce halos around targets, which may reduce the accuracy of orientation (Pesci and Teza, 2008). Additionally, moisture on targets may lead into distorted measurements with some laser scanners (Rönnholm et al., 2006). The advantage of terrestrial laser scanners is that signals can be scanned separately with more dense point spacing than other parts of the scans, because the scanner remains stable during data acquisition. Unfortunately, this method is not available for vehicle mobile mapping or airborne laser scanning, because an instrument is in constant movement. Therefore, these systems are bound to use overall point density.

In the case of airborne laser scanning, targets should be relatively large to ensure that enough laser points have received from them. Large circular targets have been used, e.g., in Toth and Grejner-Brzezinska (2005), Csanyi and Toth (2007) and Yastikli et al. (2008). Even if the accuracies were reasonable, for many laser scanning campaigns, it may not be feasible to set many targets in the field (Vosselman, 2008). In Paper **VI** and in Toth et al. (2007), pavement markings were used as targets, because white paintings are easy to distinguish from pavement using intensity values of laser data. Because the extraction of accurate points from laser scanning data is challenging, the use of linear features is recommended. Some strategies on how to extract linear features from laser scanning data are presented in Chapter 2.2.3. One alternative is to use several small surface areas as a ground reference. These reference surface areas are typically measured using differential GPS (DGPS).

In the case of image blocks, more standardized processes than with laser scanning data exist. Typically, signalized targets, natural points or linear features, such as breaklines, together with tie-point measurements are included in a bundle block adjustment. A more detailed description how to enhance a bundle block adjustment to use lines instead of points is presented, e.g., by Schenk (2004).

2.2.3   Relative orientation of images and laser data

Solving the relative orientation between laser scanning data and images is the most promising method in order to ensure the data sets to be accurately at the same coordinate system. One of the earliest examples of solving relative orientation was presented by Aldred and Bonnor (1985). The laser system was airborne and included a video camera and a single laser distance meter. Therefore, the laser measuring system produced only one single profile at a time. A video was taken simultaneously with laser profiles during the flight. Because the laser scanning campaign was carried out at the night time, the ambient light was not strong and, thus, the laser footprints were visible

on the video. The aerial image acquisition, however, was carried out at the day time. Afterwards, video frames were correlated with aerial images. After the relative orientation of the video and aerial image, the laser footprints were transferred from the video to aerial images.

Relative orientation requires that the corresponding points or features are identified from images and laser scanning data. Extracting tie features, typically, follow one of the following three basic strategies:

1. Extracting corresponding 3D features from laser scanning data and images.
2. Extracting 3D features from laser scanning data and corresponding 2D features from images.
3. Creating a virtual 2D image from a 3D laser scanning point cloud and then extracting 2D features from both laser-derived virtual image and photographic image.

The methods how basic strategies are implemented have many variations. In addition, some examples include more than one of basic strategies – one for initial orientation and another for accurate orientation.

Unfortunately, the low density of laser scanning point cloud may be an obstacle, when corresponding points or features are extracted. When laser point density is high enough, corresponding points can be manually pointed (e.g. Rocchini et al., 1999; Salemi et al., 2005; Zhao et al., 2005) with some accuracy, thus finding accurate corresponding points, especially from airborne data, is difficult or impossible (Balzavias, 1999). Even if modern airborne laser scanners can produce dense point clouds, especially if scanning is completed from low altitudes and scanning strips have large overlap, typically, the economical aspects lead to the acquisition of sparser point clouds. Therefore, use of tie-points is usually only giving an approximate orientation for more accurate orientation that uses other type of tie-features.

Extracting corresponding 3D features from laser scanning data and images

The strategy, in which 3D features are extracted from both data sources, requires stereo or multi-image measurements. Postolov et al. (1999) measured manually planar roof structures from images using photogrammetric workstation. Corresponding structures were also extracted from laser scanning data. The equations were established, in which elevation differences between two surfaces were considered as observations and unknown parameters included two horizontal shifts, rotation, scale, elevation shift and two leveling angles. The leveling angles were assumed to be small ones. The mathematical model was linearized and solved using a least squares method. However, it was pointed out that the method was not usable with steep slopes. Similar orientation approach was applied also by, e.g., McIntosh et al. (1999).

Habib et al. (2004) extracted planar patches from laser scanning data by delimiting manually potential building segments. Corresponding aerial images were use in order to assist delimiting of building segments. If planar patches of different orientations were found within a building segment, the planes were intersected in order to find straight lines. Corresponding straight lines were searched from stereo images leading to photogrammetrically measured 3D lines. 3D similarity transformation between laser scanning data and images was solved using 3D lines from both data sources. A well-written article about automatic matching 3D line sets is written by Kamgar-Parsi (2003). As an alternative to 3D lines, also 3D surfaces as tie-features have been proposed. 3D models and surfaces can be measured using both laser scanning data and images. For example, in Postolov et al. (1999) planar surfaces of sloped roofs were measured manually from aerial images. After that, the distance between corresponding laser scanning points and photogrammetrically-derived planar surfaces were minimized using least-squares method.

In Paper **III**, a laser point cloud was relatively oriented with a 3D model that was mainly measured from images. The image block consisted of both terrestrial images and an aerial image. The 3D model was extended with additional planes extracted from terrestrial laser scanning. Airborne laser scanning data was registered with the 3D model using the ICP method. Because the relationship between the 3D model and images were known, also relationship between laser scanning data and images were found. More details can be found in Chapter 4.1.

Extracting 3D features from laser scanning data and corresponding 2D features from images

If only one image is available and stereo measurements are not available, only 2D features can be extracted from the image. In such a case, 3D features can be extracted from laser data and corresponding 2D features from images. In Stamos and Allen (2000), 3D lines from terrestrial laser scanning data were extracted by intersecting adjacent planes. Corresponding 2D lines were extracted from images using the Canny operator. Relative orientation of sensors was calculated using 3D laser-derived lines and 2D image-derived lines. In addition, the same 3D lines were also used for relative orientation between adjacent laser scans. Additionally, Schenk and Csathó (2002) intersected adjacent planes in order to find straight lines. They extracted surface patches, representing roof planes, parking lots or faces of buildings, from airborne laser scanning data. Adjacent roof planes were intersected in order to find straight lines. Surface patches and straight line were considered to be sensor invariant features that can be used as tie-features. The relative orientation between laser data and aerial images was calculated using both surface patches and straight lines.

A terrestrial example was presented, for example, by Alshawabkeh and Haala (2004) who extracted edges from both terrestrial data sources. After extracting potential edges, the corresponding edges from both data sets were matched and labeled. Adjustment of

relative orientation parameters used 3D straight lines from laser scanning data and 2D lines from images.

Roux (2004) utilized a region-based segmentation to aerial images in order to extract planar segments. Planarity was checked from a set of laser scanning points, which was selected by projecting laser points to the image plane and by checking if they were inside a segment. They solved the planimetric translation automatically between aerial images and laser scanning data using quality criteria. The quality of translation was evaluated from the number of outliers when the RANSAC approach was applied to all segmented surfaces.

Extracting corresponding 2D features from laser-derived virtual images and photographic images

Many authors have decided to create a virtual 2D image from 3D laser point cloud. This task is relatively easy and if the exterior orientation of a photographic image is known, the perspective of a virtual image can be selected to be close to the perspective of a photographic image. In order to visualize projected laser point clouds on an image plane, the main alternatives are to use range- or elevation-related colorizing or intensity values. The advantage of creating a virtual 2D image from laser scanning data is that well-known image processing algorithms can be applied to the data. Such approaches lead to the extraction of 2D features from both laser scanning data and images. The connection between 2D virtual image points and the original 3D point cloud remains and can be used. However, Schenk and Csathó (2002) pointed out that, in the case of airborne laser scanning, the accuracy of extracted edges is reduced by an interpolating phase. Therefore, the accuracy of tie features may not be enough for the most accurate orientations.

Smith and Elstrom (1999) solved the relative orientation between terrestrial laser scanning and images by searching automatically for corner points from laser scanning intensity images and optical images. Only those tie-points that lie on planar surfaces were accepted. Instead of tie-points, Dias et al. (2002) extracted edges from terrestrial 2D laser intensity images and video images. The virtual 2D laser intensity images were rotated, translated and rescaled in such a way that the distance of corresponding edges in image planes were minimized. As a result, an approximate orientation was found. At the next step, interest points were searched with the Harris corner operator. Matching of corresponding tie points was carried out using cross correlation. In order to minimize the effect of lightning, the interest operator was applied to the gradient images. Mismatched corresponding points were searched and rejected by giving constraints, such as the matched points were not allowed to accumulate on small areas or the average distance of the matched points over the images should be less than a threshold.

In Umeda et al. (2004), intensity values of terrestrial 3D laser point cloud were projected into the optical image plane using initial orientation parameters. Such laser

scanning intensity images can be compared with optical images. However, because the nature of laser scanning intensity images and optical images is different, gradient images were calculated using the Prewitt operator. The criterion for a successful match was the correlation coefficient, which was calculated at several resolution stages in order to achieve more robust convergence. The process was iterative, therefore, if correlation revealed an inaccurate orientation, orientation parameters were updated and new calculations were applied.

In Zhang et al. (2005b) aerial video sequences, coarse 2D vector map data and laser scanning data were used to create textured 3D models. Initially, the camera positions were calculated using multi-view image matching and automatic aerial triangulation. Imagery included one vertical and two oblique video sequences that had over 95 % forward overlap. The image block was approximately transformed into the ground coordinate system according to a coarse 2D vector map. Tie-points between 2D vector data and images were collected manually. Initial geometric models of buildings were extracted from laser scanning data and a 2D vector map. These initial geometric models were projected onto images in order to assist image-based edge extraction. Once accurate edges were found, they were included both in the creation of a 3D model and in recalculating the bundle adjustment of images. Therefore, camera parameters were also improved at the same time as a 3D model was being constructed.

Using more than one strategies to extract tie features

In many examples, more than one of the basic extraction strategies is applied. Kurazume et al. (2002), for example, extracted edges from terrestrial laser intensity images and optical images. However, the search for corresponding tie-features was carried out using 3D edge points. In the case of laser scanning, the direct link from laser intensity image pixels and the original 3D laser point cloud remained. From the image observations, the 3D edge points were calculated. Finally, the relative orientations of all sensors were found using the robust M-estimator.

In Forkuo and King (2004), laser point clouds were projected and their intensity values were interpolated into a regular grid creating a laser intensity image. Corners were extracted from optical images and laser scanning intensity images using the Harris corner detector. Corresponding corner points were searched using the zero mean normalized cross correlation method, because it is quite robust in different lightning conditions. Remaining outliers were searched using the RANSAC algorithm. Because the connection between laser scanning intensity image pixels and original 3D laser points was known, the 3D coordinates of found corners were available. These 3D point coordinates and 2D observation from optical images were used in a bundle block adjustment, which solved relative orientation parameters for each sensor. Additionally, Paar at al. (2005) created a regular grid, but in their case it followed the known shape of a tunnel surface. Both laser scanning data and image textures were projected onto the regular grid. The relative orientation between laser scanning and images was calculated

using the method by Forkuo and King (2004). The ground coordinate system was defined by detecting signalized targets, which were measured with a total station, from laser data.

Zhang et al. (2005a) demonstrated how terrestrial laser scans and aerial imagery can be oriented relatively. For an approximate orientation, edge maps from both data sources were created and matched. The Sobel operator was applied to an aerial image in order to extract edges, whereas a grid-based range image was created from a laser scanning point cloud and potential edge points were marked, if there were significant height differences in the vicinity. Laser-derived edges were further processed by discarding short edges, fitting polylines to edge points and extending adjacent long lines until they intersected. The fine registration[2] was calculated with the ICP algorithm using information from all final edge points.

Hara et al. (2007) divided orientation into two phases in their terrestrial example. In the first phase, a robust approximation of orientations was calculated using geometrical consistencies, such as linearity, planarity, orthogonality and parallelism. Straight lines were extracted from optical images using image processing algorithms. Assuming an indoor environment, all areas that were not close to edges were considered to be planar. The approximation of relative orientations between laser scanning data and images was found by correcting orientation parameters until all 2D lines and planes from images were straight when projected on the 3D model. In addition, extracted lines and planes were expected to be either orthogonal or parallel to each other when examined in 3D. After the initial, but robust, orientation based on geometrical consistencies was solved, the final orientation was completed by projecting 3D edges from laser data onto images and by minimizing their distance to the corresponding edges extracted from images.

In addition to points, lines and planes, the shape of a group of laser scanning point clouds can be used as tie-features. In Papers **I-VI**, relative orientations were solved using large point clouds as tie-features. Because of visual interpretation and comparison, the general shape of objects, such as silhouettes and border lines, as well as single hits from details in the scene, can be used to improve the orientation. A more detailed description can be found in Chapter 3.2.

2.3   Data fusion and integrated use of images and laser scanning data

Integration of data sets does not necessarily mean fusion, but data from one sensor can be used solely for the purpose of guiding other data (El-Hakim and Beraldin, 1994). There can be different levels of data fusion, or integration, of laser point clouds and

---

[2] In most cases, the term "registration" could be replaced by the terms "orientation" or "relative orientation". However, the use of "registration" to describe a relative orientation between two 3D point clouds or surfaces has become very popular.

images depending on the desired end-product, the nature of the original data or differences in emphasis. The four main levels of integration are (paper **I**):

1. Object-level integration
2. Photogrammetry aided by laser scanning
3. Laser scanning aided by photogrammetry
4. Tightly integrated laser scanning and optical images

After all data sets are in the same coordinate system, a variety of applications exists. Currently, the main interest focuses on, e.g., automatic and semi-automatic creation of 3D models, data fusion of laser scanning and digital images, quality verification, analysis of the factors affecting the quality of laser scanning, and data classification. In following subchapter, a variety of applications using data fusion or integration of laser scanning and images are highlighted. Such applications are, e.g., advanced DTM creation, creation of ortho images, colorizing laser scanning point clouds, monoplotting, extraction of buildings or trees, data classification, creation of accurate photorealistic 3D models, automation or semi-automation, quality verification, advanced registration of adjacent laser scanning scans, and advanced detection and analysis of moving objects.

Examples of applications in which laser scanning data and images are used together

Integrated laser scanning data and images can be used for the creation of more accurate DTMs. McIntosh et al. (1999) used 3D breaklines, extracted from stereo images, to constrain the triangulation process during the creation of the DTM. In other words, individual triangles were not allowed to pass extracted breaklines. Additionally, Schiewe (2003) improved DTM creation by integrated use of airborne laser scanning and aerial images. Non-ground objects were segmented using fuzzy logic classification using both data sets. Therefore, they were able to find the terrain points more robustly.

Creating of orthoimages is a typical example, how airborne laser scanning data and images can be fused (Axelsson, 1998). Creation of orthoimages require a DTM or, in the case of true-orthoimages, a DSM. However, because laser-derived DTM or DSM does not include accurate breaklines, usually assistance of photogrammetric measurements is needed. However, orthoimages do not have to be about the ground surface. For example, Wehr and Wiedemann (1999) merged digital terrestrial images and laser scans into architectural orthoimages of facades.

Colorizing laser scanning point clouds is in many ways similar process to the creation of orthoimages. Attaching a color value from imagery to a laser scanning point cloud is nowadays available with almost all terrestrial laser scanners, but can be done also for airborne laser scanning point clouds (Paper **I**). The advantage of hybrid laser scanners is that a scanner and camera are mounted on a common rigid platform. Therefore, after a

system calibration, color values from images can be attached to the laser scanning point clouds (Abmayr et al., 2005). Scheibe et al. (2004) presented how a terrestrial laser scanning point cloud was colorized from panoramic images that were acquired with a line sensor camera. Panoramic images were acquired from many camera locations. Before colorizing, all laser scanning point clouds were merged into one 3D model. The color value of each laser scanning point was found using a ray tracing algorithm. In Paper **III**, colorizing a multi-source laser point cloud was carried out using both aerial and terrestrial images.

In monoplotting applications an image is not rectified as on orthoimage, but remains original. However, if a DSM is available, each 2D image point can have corresponding 3D coordinates. Monoplotting applications have become feasible because laser scanning provides easy access to a 3D model of a scene, where imagery is excellent for interpretation of it. Abdelhafiz et al. (2005) demonstrated a monoplotting application, in which all laser points were associated with corresponding image pixel. However, because laser point clouds were not as dense as image resolution, all image points did not have a corresponding laser scanning point. Missing depth information was interpolated in real-time. Therefore, from the users' perspective movement of the mouse cursor over a location on an image instantly made the relevant 3D coordinates visible. Ressl et al. (2006) implemented a monoplotting application, in which an operator points manually a point of interest on a high-resolution image. The corresponding 3D point was found by intersecting the light ray and the laser-derived surface patches. The sizes of surface patches were decided using a cone of interest around the light ray. Therefore, no pre-calculated 3D grid was needed and users could still obtain real-time 3D coordinate information.

Extraction of buildings or tree species usually requires classification of measured data. Forest inventory has utilized images for a long time. Laser-derived DSMs can be used for calculating tree masses both at stand level and individual tree level. Together with images, laser scanning data also enables automatic tree species classification. Even if the accuracy of automated methods are not yet at the level of manual classification, the rapidness of the method is superior when large amounts of forests are to be examined. Haala et al., (1998) used color-infrared (CIR) orthoimages and laser scanning derived nDSM for pixel-based unsupervised classification of trees, grass covered areas, buildings, and streets using simultaneously geometric and radiometric information.

In Persson et al. (2004) integrated use of laser scanning and aerial imagery was applied to classify individual trees. Individual trees and their height and crown diameter were extracted from laser scanning data. Tree crown area was projected into aerial images. The color values obtained from aerial pan-sharpened color near-infrared images (CIR) within the tree crown were examined in such a way that possible inhomogeneous illumination could be taken account. As a result, coniferous and deciduous trees were detected and separated. Morris et al. (2005) used multispectral aerial images for classification of low salt marsh vegetation. After a back-propagation artificial neural network classification, the heights of different species were determined from airborne laser scanning. Rottensteiner et al. (2004) classified buildings, trees, grass land, and

18

bare soil using Dempster-Shafer fusion. The five parameters within fusion were the height difference between DSM and DTM, the difference between the first and the last pulses, the NDVI, and two different surface roughness parameters.

Photorealistic and geometrically accurate 3D models are useful for many purposes. The size of objects can vary from small ones to complete city models. It is expected that production of 3D models will grow significantly within next decade. The requirements when creating 3D models vary according to the size and the complexity of objects. However, if a photorealistic model is needed, the presence of images is required. Further, automatic or semiautomatic creation of photorealistic 3D models, for example, usually requires data from many sources and perspectives.

In El-Hakim and Beraldin (1994) terrestrial laser scanning was used for modeling surfaces of small objects. However, edges were extracted using both laser scanning data and images. First, prominent edges were searched from laser scanning data. These edges were projected onto images to assist in searching for more accurate edge lines from images. Haala and Anders (1997) used a laser-derived DSM for assisting segmentation and recognition of buildings. The DSM was interpolated into a regular grid before potential areas including buildings were searched. By calculating Gaussian and mean surface curvatures (Besl and Jain, 1988), several surface types were classified according to the signs of surface curvatures. The method was able to extract approximate locations of edges. These edges were projected onto images in order to limit the stereo image matching area. The final edges of buildings were extracted from stereo images. Also, Schenk and Csathó (2002) applied similar approach for extracting buildings using airborne laser scanning data and aerial images. Approximate boundaries of buildings were extracted from laser scanning data. However, because of low point density, the boundaries remained fuzzy. More accurate boundaries were extracted from aerial images using the Canny edge operator. Because, both data sets were oriented at the same coordinate system, boundaries from laser scanning data could be directly replaced with boundaries measured from images. On the other hand, initial boundaries from laser data were projected to the images in order to limit the search area of the edge operator.

Deng et al. (2004) searched potential areas of buildings from laser scanning data. Aerial images were used to classify non-ground objects as buildings or vegetation. The boundaries of potential buildings were projected onto images in order to define a local neighborhood, in which more accurate edges were searched for using edge detection operators. In Park and Baek (2007), a similar approach to limit the search area from images was applied resulting in the on-line orientation of multiple scans and images. Additionally, Lee and Choi (2004) searched buildings, but they extracted building outlines from both terrestrial laser data and images. From laser data, planar patches were extracted and intersected in order to obtain edges. Correspondingly, edges were extracted from images using edge operations. By grouping edges, image-derived patches were also created. Edges and patches from both data sources were refined in order to obtain more reliable 3D models. Refined edges and patches were grouped into a polyhedron representation and textures from the images were attached to photorealistic models.

19

Sohn and Dowman (2007) demonstrated how buildings and their boundaries could be automatically detected using airborne laser scanning data and space-borne images. First, laser data was used in order to separate on-terrain and off-terrain areas. The NDVI, derived from IKONOS multispectral images, were used to reject all areas that contained vegetation. Therefore, potential areas for buildings were found. In the next step, the straight lines were extracted from images. Classified laser data assisted in deciding, whether the straight lines found belonged to building boundaries or not.

Alshawabkeh and Haala (2004) used semiautomatic photogrammetric measurements to complete gaps in 3D models acquired with terrestrial laser scanning. Typically, the reason of such gaps was occlusion of other objects or parts of objects. In addition, linear surface features, such as cracks, were extracted using image analysis.

El-Hakim et al. (2005) used aerial images to create the main shapes of building. However, they applied both terrestrial laser scanning and imagery to model details of buildings. As a typical example of an object level integration, all 3D models were created separately and registered afterwards manually using common tie points. Correspondingly, in Guarnier et al. (2006), terrestrial laser scanning data and imagery were processed separately. In their case, both data sets were transformed to the ground control points, which were measured with a total station. The main boundaries were modeled from photogrammetric data, whereas smaller details, such as reliefs, were measured using terrestrial laser scanning data.

Images provide an excellent reference that the internal geometry of laser scanning data can be compared against. Axelsson (1998) evaluated elevation accuracies by comparing photogrammetrically-derived and laser-derived DEMs. Planimetric accuracy of laser scanning data has been investigated, e.g., by comparing corners of roofs that were extracted from laser scanning data and images (Gomes Pereira and Janssen, 1999). Additionally in Papers **II-VI**, laser scanning data was examined against imagery.

Several studies have used imagery to assist more robust registering of adjacent terrestrial laser scans as an alternative to surface matching methods. Tournas and Tsakiri (2005) suggested that registration of adjacent terrestrial laser scans can be done using orthophotos. The relative orientation between a laser scanner and a camera should be known from a system calibration. An orthophoto was created from each scan. Then, corresponding points were searched from orthophotos using a cross correlation algorithm for template matching. However, only points that located on flat areas were accepted. The XY coordinates of corresponding points came from orthophoto whereas the Z coordinate was interpolated from laser scanning data. Coordinate transformation parameters were solved using six corresponding points in the object coordinate system.

Al-Manasir and Fraser (2006) used images from a terrestrial hybrid laser scanner for registering adjacent laser scans. Because relative orientation of imagery was calculated using a coplanarity model, no ground control points were needed. The scale, that remains uncertain when a coplanarity model is applied, was found in laser scanning data by measuring distances between laser scanning points that were identified also from

images. Because the system calibration of the hybrid scanner was known, also relative orientations of laser scans could be derived. When special retrotargets were placed on the scene, the orientation process could be automated and thus be an alternative to ICP-based registration of adjacent scans.

In Dold and Brenner (2006), the main tie features for registering laser scans together were planes. However, when enough planes of different orientations were not available, the registration was improved by correlating image textures that were attached to laser-derived planes. Wendt and Heipke (2006) presented simultaneous adjustment in which terrestrial optical images, laser scanning range image and normalized laser scanning intensity images were used for solving orientations of all sensors and 3D coordinates of surface patches. As usual, the adjustment required initial orientations of sensors.

Wendt (2007) registered adjacent terrestrial laser scans using imagery. Because the laser scanning data and images were acquired with a hybrid scanner, the relative orientation between a scanner and a camera was established by system calibration. Potential tie points between images from different scanner locations were searched using interest operators. Laser scanning data revealed, whether the point of interest found was located on a planar area or not. Only those points of interest were selected that lie on a plane. Images were rectified to the plane parallel to the tangent at the surface location of an interest point in focus. The purpose of rectification was to make cross-correlation more robust. The final conjugant point pairs were searched using the RANSAC algorithm in order to eliminate false matches.

Integrated laser scanning data and imagery can be utilized for detecting and analyzing moving objects. Toth and Grejner-Brzezinska (2005) estimated traffic flow using medium-format aerial images and airborne laser scanning data. Because laser scanning was acquired along a road, the velocity and moving direction of cars can be calculated according to the vehicle elongation or shortening. The true sizes of vehicles were measured using imagery.

3   Materials and methods

3.1   Laser scanning, image acquisition and field surveys

The empirical tests have been done in several test areas, which are located in Otaniemi, Espoonlahti and Kalkkinen. Each test site has been used for slightly different experiments. The test areas in Otaniemi and Kalkkinen were used for validating the developed orientation method. In addition, all test sites were used for testing potential applications. Otaniemi and Espoonlahti are sub-urban areas having both buildings and vegetation. Kalkkinen contains only forests. Figure 3 illustrates test areas with laser-derived shaded DSMs.
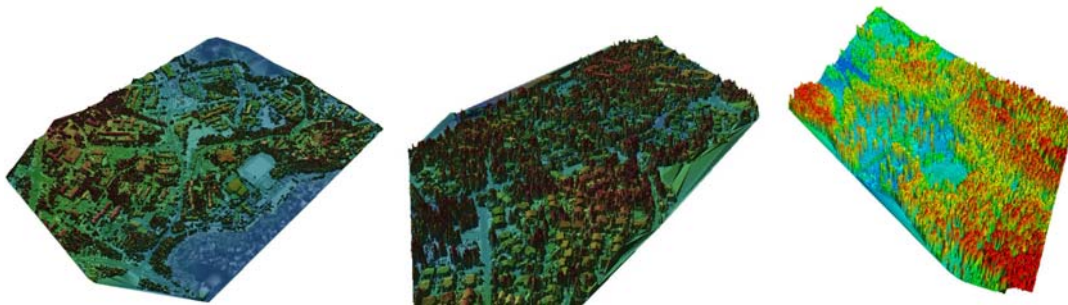
Figure 3. Shaded digital surface models of the test areas. From the left: Otaniemi, Espoonlahti and Kalkkinen.

3.1.1   Otaniemi test area

In Otaniemi several laser scanning campaigns were carried out. Toposys-1 was used in 2000 and Toposys Falcon in 2003. In 2000, the two flying altitudes were 400 and 800 meters. Resulting to point densities of 10 and 4-5 points m^{-2}. The flying height of the year 2003 scanning was 800 m with the nominal pulse density of 4 points m^{-2}. The scanning angle was ±7°, wavelength 1.54 mm and the pulse repetition rate 83 kHz. The instrument uses the fiber scanner principle (Schnadt and Katzenbeisser, 2004), which yields to a dense point cloud in the flying direction. However, as typical for fiber scanners, the point density was significantly sparser in the along-track direction than in the direction perpendicular to the flying direction. Therefore, the direction of objects at the ground has significant impact on, e.g., how accurately the breaklines could be detected.

In 2002 Otaniemi was scanned with the helicopter-borne TopEye MK I system from the flying altitudes of 200 and 550 meters. TopEye MK I system utilizes the palmer scanner principle (Wehr and Lohr, 1999), which eliminates scanning shadows along the flying direction. The flying altitude of 200 m resulted in an average point density of 2–3 points m^{-2} and an altitude of 550 m into one point m^{-2}. The scan angle of the TopEye MK I laser scanner was $\pm 20°$, wavelength 1.064 µm and the pulse repetition rate 7 kHz.

In addition to airborne laser scanning, terrestrial laser scanning was also carried out with Faro LS 880 HE80 (faro.com). Even if the scanner is able to achieve the maximum measurement rate of 12000 pulses s^{-1}, in our experiment the ¼ scanning resolution was used. The Faro LS 880 scanner is able to measure 320° vertically and 360° horizontally with a single scan. The operating wavelength of the system is 785 nm.

Several types of images were available from Otaniemi. Low-altitude aerial images were taken during the TopEye MK I campaign in 2002 with a Hasselblad digital camera based on a LightPhase CCD 3056 * 2032 resolution. At the flying altitude of 200 m, a pixel corresponded to 4.5 cm on the ground. Additionally, several terrestrial images were taken during the years 2002 and 2009. Single image, stereo images and image blocks were used. The cameras that were used were Olympus E-10 and Nikon D200 with image sizes of 2240 x 1680 and 3872 x 2592 pixels, respectively.

In addition, two panoramic images with the sizes of 9185 x 4939 pixels and 10729 x 5558 pixels were composed from seven original images taken with Olympus Camedia C-1400 L. To ensure the same perspective for all sub images, the special panoramic mount (Haggrén et al., 1998; Pöntinen, 2000) was used. The projection center of the camera was calibrated to the rotation center of the panoramic camera mount (Kukko, 2001) ensuring the concentric image acquisition.

Interior orientations were known for all images. At first, cameras were calibrated using the TKK's calibration field, but since 2006 all cameras were calibrated using iWitness software and calibration targets (Fraser and Hanley, 2004), because iWitness provided more automatic process for calibrations. The camera calibration was made each time, when a new set of images were taken, even if the camera was already calibrated earlier.

The field surveys in Otaniemi included Leica TCA 2003 total station measurements of 44 signalized targets that were used for photogrammetric measurements. In addition, about 1900 natural targets, such as pavement marks, trees, buildings, walls, and lamps were measured using both a Leica SR530 RTK GPS receiver and the total station. In Bilker and Kaartinen (2001), the accuracy of the RTK GPS was verified to be 0.015 m vertically and 0.02 m horizontally. Total station measurements included also reference tree heights. The height of 21 buildings and 102 roadside objects were measured using a Leica DISTOpro laser hand-held distance meter with an accuracy of up to ±1.5 mm.

3.1.2 Espoonlahti test area

Espoonlahti was scanned with Toposys-1 in 2000, Toposys Falcon in 2003, Optech ALTM3100 in 2005 and TopEye MKII Palmer scanner in 2006. Flying altitudes of Toposys-1 and Toposys Falcon flights were 400 and 800 meters. Optech data was acquired from 400 and 1000 meters. Optech ALTM3100 uses an oscillating mirror (Wehr and Lohr, 1999) to distribute laser beams that create a saw tooth -like pattern on the ground. The scanning repetition frequency was 100 kHz and the scanning angle was ±17 degrees.

During the TopEye MKII campaign, the flying altitude was 300 m yielding to the mean point density of 16.6 points m^{-2}. In addition to relatively high point density, the full waveform data was available. The sample interval of the waveform was 1 ns, corresponding to approximately a 15 cm resolution in the beam direction. As a palmer scanner, the scan angle varied between 9 and 25 degrees. The length of a single laser pulse was 5 ns and beam divergence 1 mrad.

3.1.3 Kalkkinen test area

The test area in Kalkkinen was scanned with a Toposys-1 laser scanner in 2000. The flying altitude was 400 m resulting in the average point density of 10-20 points m^{-2}. Two terrestrial panoramic images were created with dimensions of 1539 x 3302 pixels and 1484 x 2293 pixels using the same method as described earlier. As a ground reference and check points, a set of signalized points were measured using a total station.

3.2 Interactive orientation

Software for demonstrating interactive orientation of laser scanning data and images was developed. Interactive orientation was a solution to overcome difficulties in extracting conventional features, such as points, lines and surfaces, from laser scanning data. During interactive orientation the laser point cloud is superimposed onto an image or an image block using current orientation information. Superimposing requires a transformation from 3D ground coordinates to camera coordinates. The transformation can be calculated using collinearity equations:

Superimposing of a 3D laser point cloud requires a known camera model. All images fulfilled the condition of central perspective. Therefore, each laser point is transformed from 3D ground coordinates to camera coordinates (x, y).

$$x = x_0 - c\frac{r_{11}(X - X_0) + r_{21}(Y - Y_0) + r_{31}(Z - Z_0)}{r_{13}(X - X_0) + r_{23}(Y - Y_0) + r_{33}(Z - Z_0)}$$

$$y = y_0 - c\frac{r_{12}(X - X_0) + r_{22}(Y - Y_0) + r_{32}(Z - Z_0)}{r_{13}(X - X_0) + r_{23}(Y - Y_0) + r_{33}(Z - Z_0)} \qquad (1)$$

where c is a principle distance, a point (X_0, Y_0, Z_0) is the projection center of a camera, (X, Y, Z) is a 3D ground point, terms $(r_{11}...r_{33})$ are elements of a 3D rotation matrix, and (x_0, y_0) is the location of a principal point.

Collinearity equations assume the case of an ideal central perspective, which is not realistic because of lens distortions. Therefore, the amount of existing lens distortion should be taken account, before plotting the point onto an image. Alternatively, the lens distortions can be eliminated from an image beforehand, which unfortunately requires resampling and interpolation of the image.

Even if several variations for correcting lens distortions exist, one of the most commonly used models was originally formulated by Brown (1971). The model includes radial and decentering corrections. The amount of radial distortion (Δr) depends on the distance (r) from the distortion center according to the equation:

$$\Delta r = K_1 r^3 + K_2 r^5 + K_3 r^7 + ... \qquad (2)$$

In most cases, the first three coefficients (K_1, K_2 and K_3) are sufficient for correcting radial distortion, because the higher order terms are insignificant. When radial correction is divided into two components along the x and y axes of the camera coordinate system, the amount of corrections (Δx_{radial}, Δy_{radial}) become:

$$\Delta x_{radial} = x_c(K_1 r^2 + K_2 r^4 + K_3 r^6)$$

$$\Delta y_{radial} = y_c(K_1 r^2 + K_2 r^4 + K_3 r^6), \qquad (3)$$

where

$$x_c = x - c_x, \qquad y_c = y - c_y, \qquad r^2 = x_d^2 + y_d^2$$

A point (c_x, c_y) is the distortion center. If the distortion center unites with the principle point, the coordinate (x_c, y_c) is equal to the result (x, y) from the collinearity equations (1).

Decentering distortions are typically much smaller than radial distortions. In Brown's model decentering distortion is corrected:

25

$$\Delta x_{decentering} = \left[P_1(r^2 + 2x_c^2) + 2P_2 x_c y_c\right]\left[1 + P_3 r^2 + ...\right]$$
$$\Delta y_{decentering} = \left[P_2(r^2 + 2y_c^2) + 2P_1 x_c y_c\right]\left[1 + P_3 r^2 + ...\right] \quad (4)$$

Usually, only coefficients P_1 and P_2 are needed to achieve sufficient accuracy. When radial and decentering lens distortion corrections are combined, the corrected camera coordinates ($x_{corrected}$, $y_{corrected}$) are:

$$x_{corrected} = x + \Delta x_{radial} + \Delta x_{decentering}$$
$$y_{corrected} = y + \Delta y_{radial} + \Delta y_{decentering} \quad (5)$$

In the case of digital images, camera coordinates are typically transformed further into an image coordinate system. Typical selection for image coordinate system is to place the origin at the left upper corner and to let x axis grow to the right and y axis to the down.
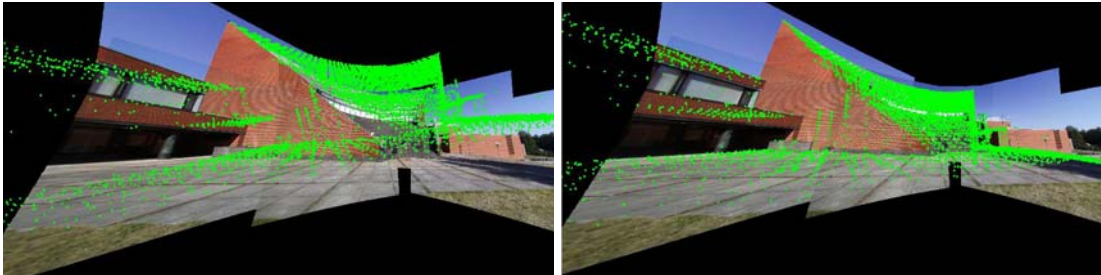
Figure 4. Superimposing laser scanning data onto the images illustrates how well the orientation has succeeded.

Superimposing typically reveals visually if laser data fits with images (Figure 4). If any misalignment is detectable, tools for improving orientations are required. In software, the exterior orientation parameters are adjustable. Exterior orientation parameters include location of the projection center (X_0, Y_0, Z_0) in the ground coordinate system and three rotations. The selection of three rotations depends on image types. In photogrammetric applications omega (ω), phi (φ), kappa (κ) rotations are typically preferred, if aerial images are involved. These rotations are done around the coordinate axes of the camera coordinate system. However, this rotation system is not very intuitive if used during interactive orientation. In other words, it is usually not easy to predict how changes to rotations will change the relative orientation between a laser point cloud and an image. Much more intuitive selections for rotations are azimuth (α), tilt (ν) and swing (κ) (Figure 5), for example.
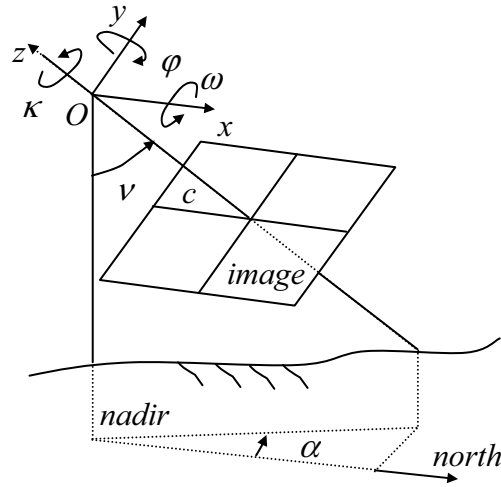
Figure 5. Azimuth, tilt and swing (α, v, κ) rotations are usually more intuitive than rotations around the axes of the camera coordinate system (ω, φ, κ).

Even if the physical rotation system can be selected freely, the final result is always a 3D rotation matrix (R), which is required for collinearity equations.

$$R = \begin{bmatrix} r_{11} & r_{12} & r_{13} \\ r_{21} & r_{22} & r_{23} \\ r_{31} & r_{32} & r_{33} \end{bmatrix}$$

The elements of 3D rotation matrix can be derived for both rotation systems. In this case, all rotations defined to be positive to the clock-wise direction and coordinate systems are assumed to be right-handed.

$$r_{11} = \cos\varphi\cos\kappa \qquad\qquad r_{11} = \cos\alpha\cos\kappa - \sin\alpha\cos v\sin\kappa$$

$$r_{12} = -\cos\varphi\sin\kappa \qquad\qquad r_{12} = -\cos\alpha\sin\kappa + \cos\alpha\cos v\cos\kappa$$

$$r_{13} = \sin\varphi \qquad\qquad r_{13} = \sin\alpha\sin v$$

$$r_{21} = \cos\omega\sin\kappa + \sin\omega\sin\varphi\cos\kappa \qquad\qquad r_{21} = \sin\alpha\cos\kappa + \cos\alpha\cos v\sin\kappa$$

$$r_{22} = \cos\omega\cos\kappa - \sin\omega\sin\varphi\sin\kappa \qquad\qquad r_{22} = -\sin\alpha\sin\kappa + \cos\alpha\cos v\cos\kappa \qquad (6)$$

$$r_{23} = -\sin\omega\cos\varphi \qquad\qquad r_{23} = -\cos\alpha\sin v$$

$$r_{31} = \sin\omega\sin\kappa - \cos\omega\sin\varphi\cos\kappa \qquad\qquad r_{31} = \sin v\sin\kappa$$

$$r_{32} = \sin\omega\cos\kappa + \cos\omega\sin\varphi\sin\kappa \qquad\qquad r_{32} = \sin v\cos\kappa$$

$$r_{33} = \cos\omega\cos\varphi \qquad\qquad r_{33} = \cos v$$

The 3D rotation matrix also plays a key role when the camera system is shifted during an interactive orientation. A trivial case, in which shifts are done along the coordinate

27

axes of the ground coordinate system, is not always practical enough for interactive orientation. More intuitive is to have tools for shifting a camera to the directions of the axes of the camera coordinate system. From a 3D rotation matrix we are able to find unit vectors that describe the directions of the axes of the camera coordinate system in the ground coordinate system. The equations for shifting the projection center of the camera (X_0, Y_0, Z_0) can be written (Gruber, 2000):

$$\begin{bmatrix} X_0 \\ Y_0 \\ Z_0 \end{bmatrix}_{x-shifted} = n \begin{bmatrix} r_{11} \\ r_{21} \\ r_{31} \end{bmatrix} + \begin{bmatrix} X_0 \\ Y_0 \\ Z_0 \end{bmatrix}_{original} \quad , \quad \begin{bmatrix} X_0 \\ Y_0 \\ Z_0 \end{bmatrix}_{y-shifted} = n \begin{bmatrix} r_{12} \\ r_{22} \\ r_{32} \end{bmatrix} + \begin{bmatrix} X_0 \\ Y_0 \\ Z_0 \end{bmatrix}_{original} \quad ,$$

$$\begin{bmatrix} X_0 \\ Y_0 \\ Z_0 \end{bmatrix}_{z-shifted} = n \begin{bmatrix} r_{13} \\ r_{23} \\ r_{33} \end{bmatrix} + \begin{bmatrix} X_0 \\ Y_0 \\ Z_0 \end{bmatrix}_{original} \quad . \quad (7)$$

The parameter n in equations defines the amount of shift in the ground coordinate system units. If these shifts are used during an interactive orientation, the laser point cloud always seems to move up, down, left, right, forward, or backward in respect to the image.

An interactive orientation can be done by changing only shifts and rotations. However, a possibility to use an anchor point is significantly improving the practicality of the method (Figure 6). At the beginning of the interactive orientation it is common that only some part of the laser data is close to corresponding features in the image and the rest are misaligned because of incorrect orientation. By setting an anchor point, an interactively applied shift causes automatically corresponding rotation to the attitude of the camera in order to fix those laser points that are already close to correct location in the image plane. In Paper **II**, an iterative method for solving rotations was presented.
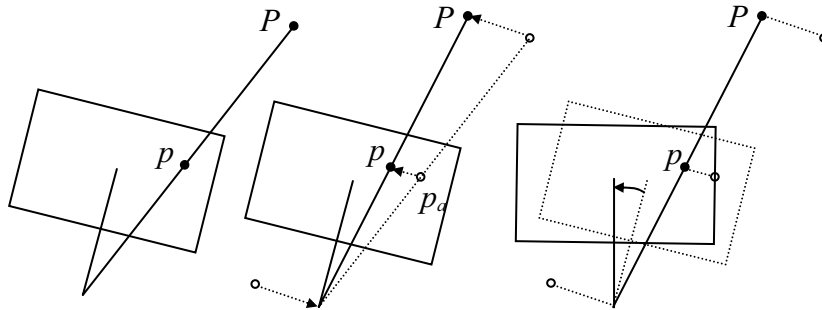
Figure 6. The location of an anchor point on the image remains because an interactive shift of the projection center is compensated automatically by corresponding rotations. (from Paper **II**)

All available laser scanning data or, preferably, selected sub-sets of it can be used during an interactive orientation. The type of distinguishable corresponding features between laser data and images is case sensitive. However, it is typical that, after the initial orientation is already improved, it is close to the correct values, and superimposing laser data onto an image reveals small details, such as lamp poles, fences, chimneys, antennas etc. This kind of details usually provides more information for orientation. However, without the support from images, it would be difficult to distinguish small objects from outliers. After all, small objects may have only one or just couple of hits within laser scanning data. In some cases, even vegetation can be a useful feature in assisting with interactive orientation. Because vegetation is not stable, the weather conditions, especially wind, should be carefully taken into account.
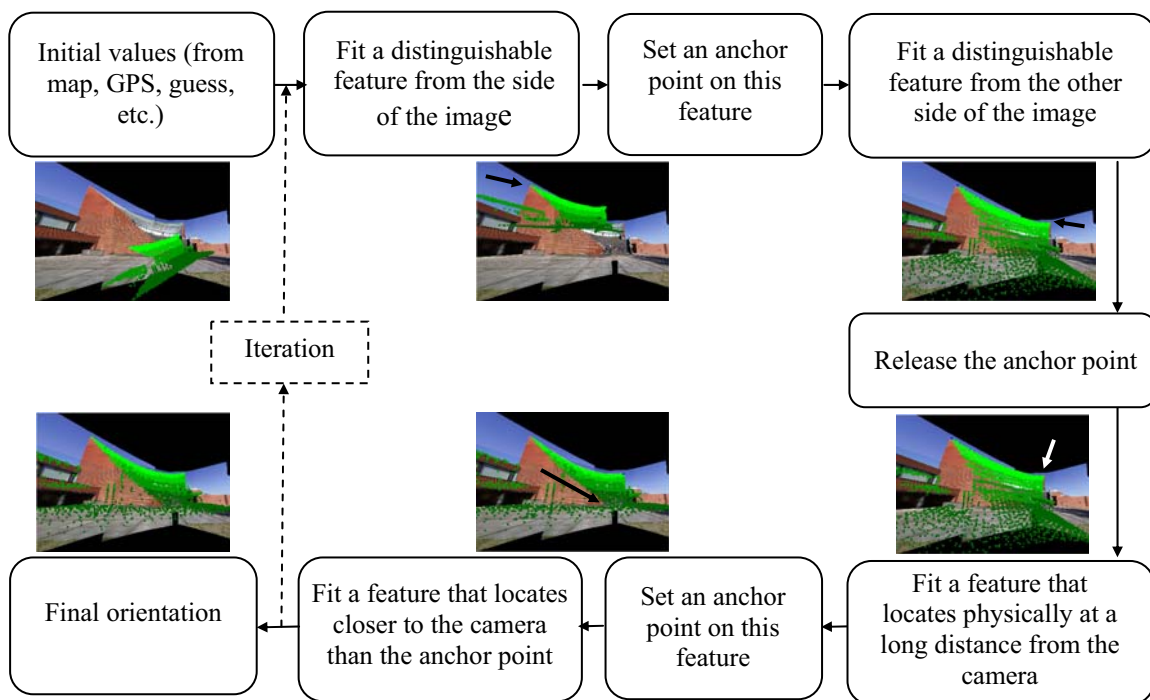
Figure 7. Suggested workflow for interactive orientation of a single image and laser point cloud. (from Paper **III**)

One suggestion on how to apply the workflow for an interactive orientation of a single image is illustrated in Figure 7. Ideally, within the field of view (FOV) there should be sufficient amount of distinguishable features both close to and far from the camera. In addition, it is advantageous if tie features can be found from the both sides of the FOV. Even if all available features are usable to find both the rotations and the shifts of a camera, features with different distances from the camera especially assist in finding correct rotations for the orientation. Correspondingly, vertically distributed features especially assist in finding the correct location along the optical axis. An interactive orientation is an iterative process. At first, a coarse orientation is made and after that more tie features can be distinguished, which can be used in the next orientation round

in order to improve orientation. At some point, the laser point cloud fits with the image and no improvement can be found.

The FOV of a single image is usually relatively narrow, if a normal lens is used during the image acquisition. Because a narrow FOV prevents tie features in the horizontal direction to be far apart, the possibility of finding the correct location along the optical axis is reduced. One solution to overcome this is to use panoramic images. Another solution is to have more than one image taken from different perspectives. If images have been taken by the means of a normal case of stereo imaging, images can be seen in 3D. On the other hand, if images have been taken from different sides of the object, more information about the object can be seen. In the most advanced case, a block of images are oriented with laser scanning data.

In order to use an image block instead of a single image during an interactive orientation, the relative orientations of all images must be solved. Typically, orientations are calculated in a bundle block adjustment (Triggs et al., 1999), for which task several types of photogrammetric software are nowadays available (e.g. Wiedemann et al., 2001). In the present study, the iWitness software (Fraser and Hanley, 2004) was used for image orientations. Basically, an interactive orientation using an image block is very similar to the case of a single image. The difference is that if one image of the block is rotated or shifted, all other images are moving along. The case of rotations is more complex than that of shifts, because a rotation of an active image causes both shifts and rotations of all other images.
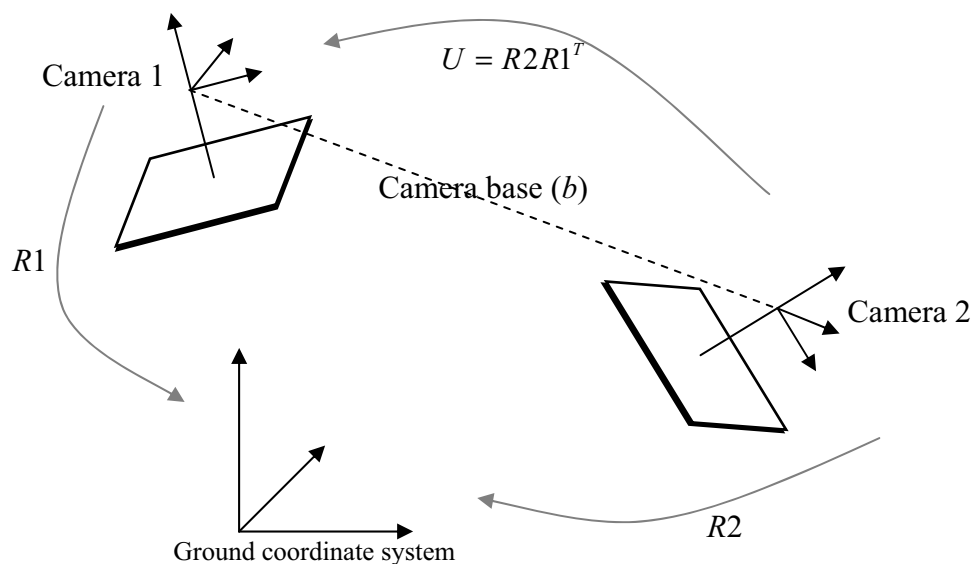
Figure 8. With 3D rotation matrices $R1$, $R2$ and U camera coordinate observations can be rotated to a coordinate system parallel to the target coordinate system. Because 3D rotation matrices are orthogonal, inverse matrices can be calculated with matrix transposes. (from Paper **III**)

The new 3D rotation matrix for any other image in the block can be calculated using the following procedure. Because exterior orientations of images and, therefore, 3D rotation matrices for each camera location are available from the bundle block adjustment, the relative rotation matrix ($U_{relative}$) between two cameras can be derived (Figure 8):

$$U_{relative} = R2_{original} R1_{original}^T \qquad (8)$$

In this example, the active camera is the first one and therefore the rotation matrix ($R1$) is attached to it. The second rotation matrix ($R2$) is attached to the camera that is moving along if the orientation parameters of the first camera are changed. Next, the camera base (b) between two cameras is calculated using the projection centers of the cameras $P1_0$ and $P2_0$:

$$b_{ground} = P2_{0\_original} - P1_{0\_original} \qquad (9)$$

As a result, the camera base is expressed at the ground coordinate system. In order to attach the image base to the active image, the camera base is converted into the camera coordinate system of the active camera.

$$b_{camera1} = R1_{original}^T b_{ground} \qquad (10)$$

The relative rotation matrix ($U_{relative}$) and the camera base ($b_{camera1}$) are invariants, when an active image is rotated or shifted. When an active image is interactively rotated, a new 3D rotation matrix $R1_{new}$ is obtained as a result. By using the new rotation matrix and an invariant relative camera base, the new location of the projection center of the second camera can be calculated:

$$P2_{0\_new} = R1_{new} b_{camera1} + P1_{0\_original} \qquad (11)$$

Similarly, the new rotation matrix for the second image can be calculated using the new 3D rotation matrix of the first image and the invariant relative rotation matrix ($U_{relative}$):

$$R2_{new} = U_{relative} R1_{original} \qquad (12)$$

The suggested strategy for completion of interactive orientation using an image block begins with the same workflow as was presented in the case of a single image (Figure 7). However, this workflow is followed only to obtain an initial orientation that is already close to the correct one. Therefore, there is no need to try finding an accurate orientation at this stage. After the initial relative orientation is solved, it is recommended to set one image as a master image and monitor the effects of changing orientation parameters of the master image from other images. If any rotation differences exist between laser scanning data and the image block, the use of an anchor point assists the orientation, as with the case of a single image. In the optimal case, the

image block includes such camera stations whose viewing directions are close to perpendicular to each other. However, in practice, it is seldom possible to arrange image acquisitions in such a way. If the images are not taken perpendicularly, in some cases, it may be difficult to predict how changing rotation of the master image affects to the orientations of other images. In order to avoid, corrections at the time that are too large, an iterative approach, in small steps, towards the correct solution is recommended. Finally, the solution becomes accurate enough that no misalignment of laser scanning data is detectable from any images within the image block.

In some cases, images and laser scanning data have no rotation differences, but only shifts. This changes the strategy for deriving the interactive orientation of an image block. All images can be selected as a master image in turn. From each image, misalignment of laser scanning data is corrected only along the x and y axes of the image coordinate system. Using images taken from several viewing directions, this leads iteratively to the correct solution when orientation cannot be improved any more from any images.

In developed software, an interactive orientation changes exterior orientations of images. In many cases, however, it is easier to obtain an image block oriented into the ground coordinate system than laser scanning data. Therefore, a transformation is needed, which applies a transformation to laser scanning data and image orientations can be restored to original ones. Before any rotations can be applied to laser scanning data, all laser points ($x=[X\ Y\ Z]^T$) must be shifted in such a way that the origin of the coordinate system is at the projection center of a camera after an interactive orientation (P_{0_after})

$$x_{shifted} = x_{original} - P_{0\_after} \qquad (13)$$

In order to know how much the interactive orientation changed, the 3D rotation matrix of the active image, Equation (8), can be applied in such a way that *R1* is a 3D rotation matrix after interactive orientation and *R2* is an original 3D rotation matrix. Similarly, the shifts between an interactively oriented image and original location can be solved:

$$t = \begin{bmatrix} X_0 & Y_0 & Z_0 \end{bmatrix}^T_{original} - \begin{bmatrix} X_0 & Y_0 & Z_0 \end{bmatrix}^T_{after} = \begin{bmatrix} dX_0 & dY_0 & dZ_0 \end{bmatrix}^T \quad (14)$$

Rotations and shifts can be applied to the laser scanning point cloud:

$$x_{transformed} = Ux_{shifted} + t \qquad (15)$$

The origin of the coordinate system is still at the projection center of the active image. Therefore, the laser point cloud still requires to be shifted to the ground coordinate system

$$x_{final} = x_{transformed} + P_{0\_after} \qquad (16)$$

4 Results

4.1 Accuracy of interactive orientations

The first experiment for analyzing the accuracy of the interactive method was carried out in the Kalkkinen test area. A set of signalized points was placed on the scene and measured with a total station. These 3D points from total station measurements were used as a point cloud for an interactive orientation. An experiment included two terrestrial panoramic images, which established a stereo image pair. Using signalized points, the exterior orientations of images were solved also using least-squares adjustment, thus no additional relative orientation was performed. The number of visible ground control points was six from the left image and five from the right image. Image orientations for both images were solved separately using interactive orientation using ground control points. The results of computational and interactive orientation were compared (Table 1). For the left image, two computational orientations were calculated, because superimposing ground control points onto the image during interactive orientation revealed two inaccurate points. Therefore, in the second orientation, only four ground control points were included.

Table 1. Differences of orientation parameters between computational and interactive orientation methods. The first orientation of the left image was calculated using all control points. For the second orientation, inaccurate control points were removed.

	ΔX	ΔY	ΔZ	Δω (gon)	Δφ (gon)	Δκ (gon)
Left Image 1	-0.043 m	0.017 m	0.005 m	0.103	-0.052	0.204
Left Image 2	0.014 m	-0.017 m	-0.004 m	-0.043	0.015	-0.085
Right Image	-0.053 m	-0.012 m	0.019 m	-0.027	-0.023	0.050

Using photogrammetric forward intersection, four check points were measured from stereo images. Photogrammetric measurements were applied for three different cases. In first case, the image orientations were achieved with a least-squares method using all available ground control points. In the second case, two inaccurate ground control points were removed before calculating exterior orientations. The third orientation was completed using an interactive method. The results from each case were compared with total station measurements (Table 2).

Table 2. Differences between check points and stereo measurements. When terrestrial images are used, the errors of orientations cause larger errors in stereo measurements, if the point is located far from the camera.

Point	1st computational orientation, all control points			2nd computational orientation, inaccurate control points eliminated			Interactive orientation, all control points			Point distance from 1st camera
	ΔX (m)	ΔY	ΔZ	ΔX	ΔY	ΔZ	ΔX	ΔY	ΔZ	(m)
1	0.010	0.003	-0.005	-0.007	-0.001	0.008	-0.019	-0.014	0.007	27.69
2	0.052	0.066	0.010	0.013	0.015	0.008	-0.054	-0.082	0.043	52.44
3	0.159	0.111	-0.022	-0.002	0.011	0.011	0.060	0.030	-0.019	56.26
4	0.658	0.628	-0.039	0.023	0.011	0.005	0.157	0.112	-0.038	98.77
Mean	0.220	0.202	-0.014	0.007	0.009	0.008	0.036	0.012	-0.007	
RMSE	0.340	0.321	0.023	0.014	0.011	0.008	0.089	0.071	0.030	

In the Otaniemi test area, several experiments were carried out in order to understand better, how interactive orientation performs. The first experiment included two terrestrial panoramic images, which were oriented interactively with a georeferenced laser point cloud. Camera locations were also measured using RTK GPS. Comparison between RTK GPS measurements and interactively solved camera locations is presented in Table 3.

Table 3. Comparison between RTK reference measurements and interactively oriented camera locations.

	ΔX_0	ΔY_0	ΔZ_0
Image 1	-0.215 m	-0.141 m	0.012 m
Image 2	-0.129 m	-0.078 m	-0.038 m

Comparison with RTK GPS observations did not provide information about the rotation differences. Therefore, a new experiment was arranged (Figure 9). Instead of using a single image at the time, a block of images were included. The reference was obtained by creating a georeferenced 3D model from photogrammetric measurements and terrestrial laser scanning. The reference orientation of the image block was solved using the iWitness software resulting in an overall accuracy of 1.3 cm. The estimated accuracy of image referencing was 0.72 pixels.

The airborne laser scanning data was registered with a 3D model using the ICP method implemented in Geomagic Studio 9. After the registration, the software reported an average deviation of 2.5 cm. The result was verified visually by superimposing the laser scanning point cloud onto the image. Visual inspection did not reveal observable misalignment between laser scanning data and images. As a result, the laser scanning data and all images within the image block were at the same coordinate system.

In order to perform interactive orientation, some images from the image block were selected. The relative orientations of images were preserved, but the exterior orientation of the image block was changed arbitrarily. Interactive orientation was carried out several times between image blocks and laser scanning data. Because georeferenced laser scanning data was used as a reference, the results from the interactive orientation were comparable with original exterior orientations of the image block.
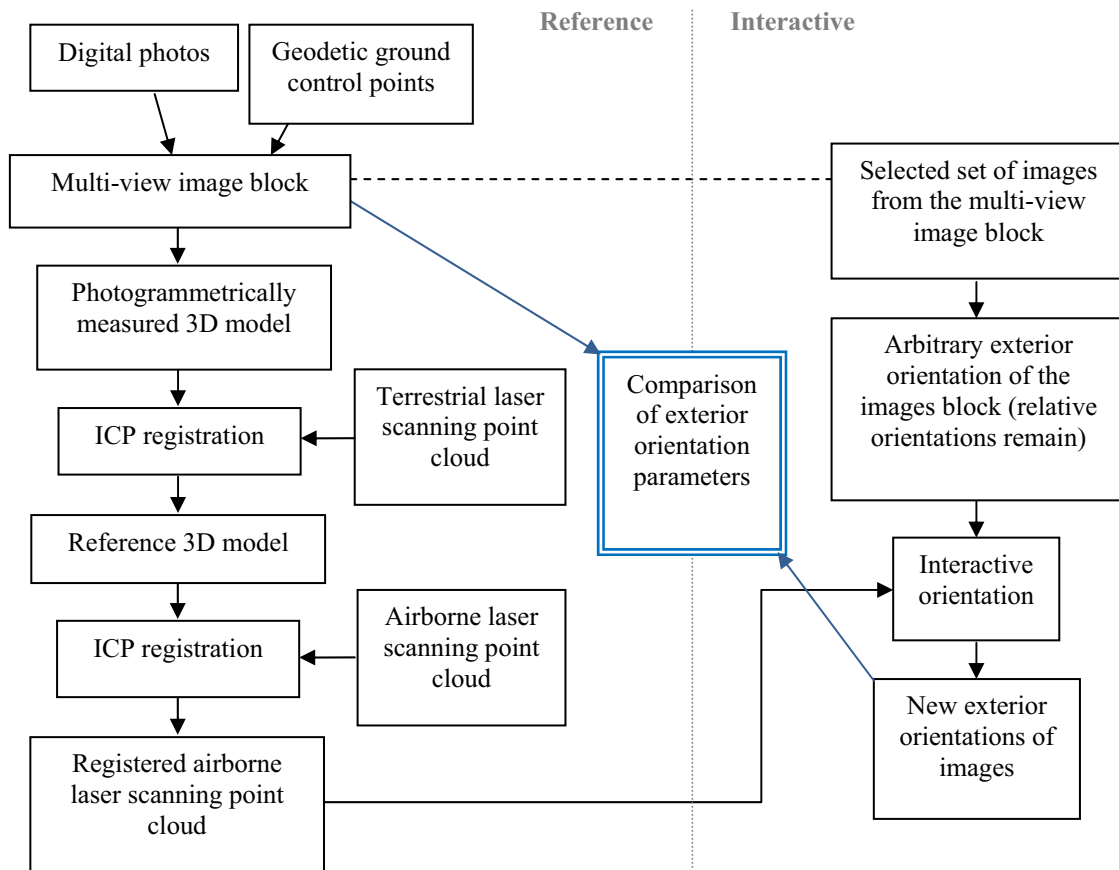
Figure 9. The workflow for comparing all exterior parameters between interactive orientation and reference orientations. (from Paper **III**)

The first experiment of interactive orientation of an image block included an aerial image and a terrestrial panoramic image. Interactive orientation was repeated 8 times starting each time from a new arbitrarily chosen exterior orientation of the image block. The results of comparison are illustrated in Table 4.

Table 4. Differences of exterior orientation parameters (interactive orientation – reference). The interactive orientation was applied using simultaneously a terrestrial panoramic image and an aerial image, whose relative orientation was known. Statistics were calculated from 8 individual orientations.

	Aerial image					
	X (cm)	**Y (cm)**	**Z (cm)**	ω **(deg)**	φ **(deg)**	κ **(deg)**
Average	-8.1	2.2	-1.1	-0.062	-0.012	0.046
Std	10.6	15.4	2.5	0.064	0.041	0.038
Max	20.0	30.5	5.6	0.194	0.069	0.106
	Panoramic image					
	X (cm)	**Y (cm)**	**Z (cm)**	ω **(deg)**	φ **(deg)**	κ **(deg)**
Average	-3.1	-2.8	-0.6	-0.005	-0.063	0.043
Std	5.1	7.2	1.8	0.055	0.056	0.033
Max	10.2	18.5	4.1	0.101	0.176	0.065
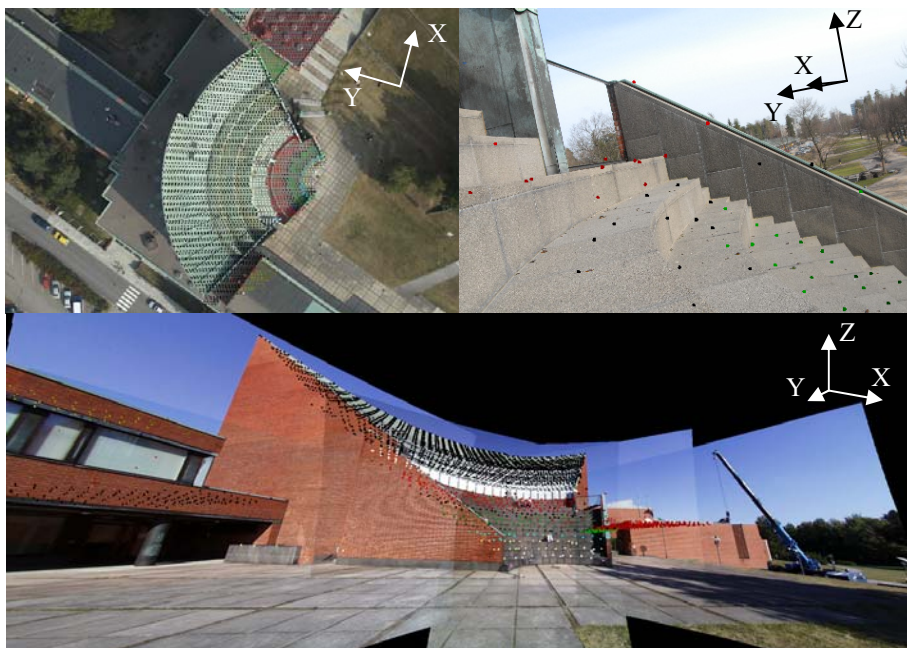
Figure 10. Laser scanning data, which was used for interactive orientation, superimposed onto aerial, close-range and panoramic images. The color-coding illustrates the heights of laser points. The coordinate axes illustrate the approximate directions of the ground coordinate system. (from Paper **III**)

The amount of images in the block was increased by including a close-range image. The close range image was taken with normal 18 mm lens and therefore the FOV of the image was not very large. However, the optical axis of the image was almost

perpendicular to both the aerial image and the panoramic image (Figure 10). The results of comparison with reference orientations are in Table 1.

Table 5. Differences of exterior orientation parameters (interactive orientation – reference). The interactive orientation was applied using simultaneously a close-range normal-angle image, a terrestrial panoramic image and an aerial image, whose relative orientations were known. Statistics were calculated from 8 individual orientations.

	X (cm)	Y (cm)	Z (cm)	ω (deg)	φ (deg)	κ (deg)
			Aerial image			
Average	-9.6	1.5	-0.4	-0.033	-0.017	0.038
Std	7.4	12.0	1.2	0.031	0.036	0.021
Max	20.9	16.3	2.4	0.097	0.065	0.065
			Panoramic image			
Average	0.6	0.7	-1.2	0.024	-0.017	0.045
Std	2.6	0.4	1.4	0.035	0.022	0.028
Max	6.8	1.3	2.8	0.065	0.046	0.078
			Close-range image			
Average	1.2	0.3	-0.6	-0.034	0.022	0.008
Std	2.3	0.2	0.8	0.062	0.023	0.050
Max	6.5	0.6	2.0	0.105	0.054	0.097

The last experiment simulated the case, in which the laser scanning data is already well leveled and only shifts are included. During the interactive orientation, the same images as in the previous case were used. The results are presented in Table 6.

Table 6. Differences of shifts (interactive orientation – reference). Because there were no rotation differences between laser scanning data and the image block coordinate system, the differences of shifts were the same for all images. Statistics were calculated from 8 individual orientations.

	X (cm)	Y (cm)	Z (cm)
		Image block	
Average	0.7	0.3	-0.9
Std	1.2	0.3	0.5
Max	2.6	0.6	1.8

4.2 Experiments on data fusion and integrated use of laser scanning and images

Several authors (e.g. Hyyppä and Inkinen, 1999; Persson et al., 2002; Gaveau and Hill, 2003; Leckie et al., 2003; Yu et al., 2004; Wang et al., 2009) have reported that airborne laser scanning data typically underestimates tree heights. In our research, presented in Paper **IV**, this phenomenon was verified by comparing tree heights derived from laser scanning data with total station observations. In addition, some example trees, whose heights were underestimated according to our measurements, were photographed. The aim of taking these terrestrial images was to obtain detailed information about the cause of underestimation of tree heights by laser scanning. The images were selected in a way that nearby the trees there were also solid structures, such as buildings. Relative orientation between laser data and images was solved using interactive orientation. After the interactive orientation, the laser data was examined against the images (Figure 11). Example cases proved that, typically, laser data has not been dense enough to obtain measurements from the very top of the example trees.

Figure 11. Leaf-on laser scanning has not found the highest top of the birch (left). The black spot indicates the actual treetop and the white ones represent laser data. The perspective causes a misunderstanding of the heights, because the treetop is observed from a worm's-eye view. The distance between the highest laser point and the actual treetop is 1.37 meters. Spruce is measured with about 50 pulses per square meter (right). Part of the spruce is shadowed by surrounding aspens. (from Paper **IV**)

An example, which aimed to demonstrate usability of images for understanding the temporal changes that has happened between two batches of laser scanning data acquired in different years, was illustrated in Paper **II**. The two batches were separately oriented interactively with an oblique image. After the interactive orientation, the higher parts of both laser data sets were superimposed simultaneously into the images (Figure 12). Experiment revealed that visually, it is relatively simple to detect changes and to understand, which objects were not anymore visible. In addition, the differences of two

different laser scanners are illustrative. For example, laser scanners have behaved differently when interacting with street signs and their supporting framework.

Figure 12. White spots are scanned from 800 m with a pulse repetition rate of 83 kHz (airborne TopoSys-1) and black points are scanned from 200 m at a rate of 7 kHz (helicopter-borne TopEye). (from Paper **II**)

An example, which also demonstrated detection of temporal changes, was illustrated in Paper **I**. In this case, only one set of laser scanning data was available. However, the images were taken at intervals of half a year. Images and laser data were interactively oriented together. Image series in Figure 13 demonstrates how a temporary structure from the roof of the building has been removed in 6 months. From the laser point cloud only, the existence of temporal structure is undetectable. However, from the image that was taken simultaneously with laser scanning, the nature of this structure is already understandable. Finally, when integrating an image taken after 6 months with laser scanning data, the difference of data sets is obvious, because the temporal structure has been removed.

Figure 13. a) Perspective view of the ALS point cloud b) ALS data is integrated with the terrestrial image c) after half a year, the temporary structure was removed from the roof. (from Paper **I**)

In Paper **I**, laser scanning data has been interactively oriented with a stereo image pair (Figure 14). Stereo vision provides an extended possibility for examining the behavior of laser data and to interpret even small details of the scene. In addition, even if images

are examined monoscopically, stereo images assist in finding more accurate locations for cameras, especially in the forward or backward directions.
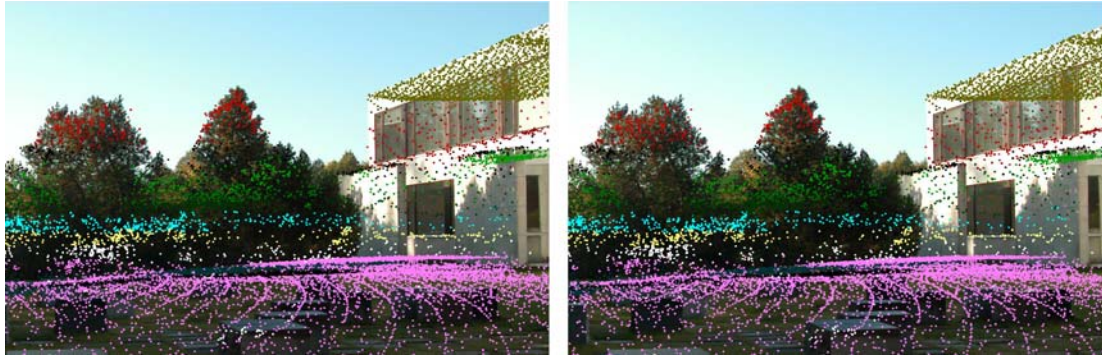
Figure 14. Cross-eye stereo images with a superimposed laser scanning point cloud (TopEye MK-II). (from Paper **I**)

In Paper **III**, laser point clouds from multiple sources were colorized with RGB colors (Figure 15). Laser scanning data included both airborne and terrestrial scans. Colors of some vertical structures were taken from terrestrial images whereas other structures were colorized from an aerial image. Integrating data from multiple sources and from several viewing perspectives requires successful orientations of all data sets. However, this method allows completing areas that have been in shadows from another scan or image. In addition to RGB colorized laser point clouds, also other color band combinations were experimented with. In Paper **I**, a laser scanning point cloud was colorized with false-colors from UltraCam-D's digital aerial image (Figure 16). In this case, the difference between vegetation and non-vegetation is illustrative.
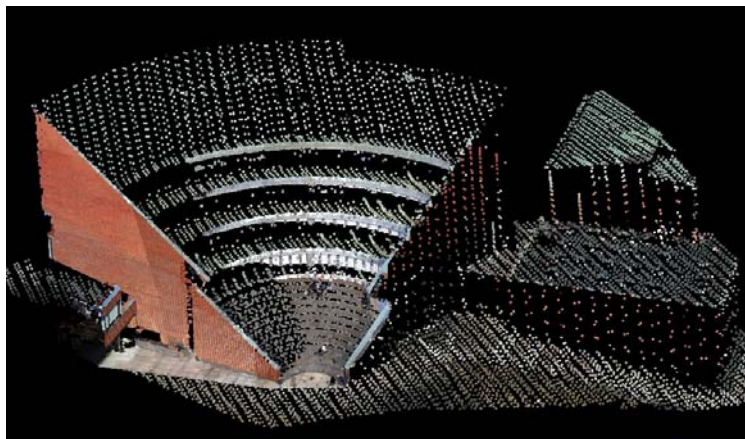
Figure 15. After the registration, terrestrial and airborne laser scanning data were integrated. Laser scanning points were colorized using both aerial images and terrestrial panoramic image.
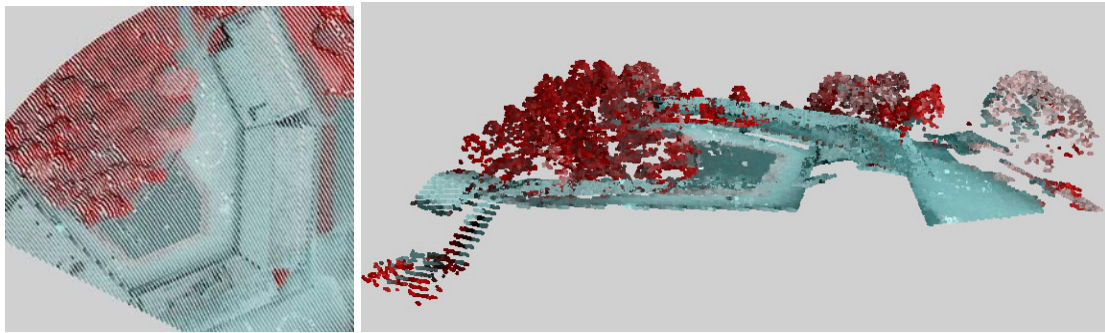
Figure 16. False-colors from UltraCam-D's digital aerial images have been associated with the laser point cloud. Left: the point cloud in ortho projection. Right: perspective side view.

Full waveform laser scanning data were examined in Paper **V** by superimposing it onto the terrestrial images (Figure 17), which were taken from different perspectives. The interactive orientation, however, was completed using the first pulse laser scanning data. To make orientation more robust, images from different perspectives were used simultaneously during the interactive orientation. Because the wind was quite strong during the data acquisitions, laser data from the tree top is not precisely aligned with images. Therefore, mainly more stable objects, such as a building, fence and lamp poles, were used as a tie features during the interactive orientation.

Figure 17. The full-waveform superimposed onto images. The difference in the viewing angles of the images is close to 90 degrees.

Images at the background of superimposed laser scanning data were used to assist manual selection of such laser echoes that has been hit the tree trunk. The image sequence in Figure 18 illustrates how a set of laser points was first selected from the first image. As a result, a cross section of laser points is contained within a selection. These points are superimposed onto the next image, whose viewing direction is almost perpendicular to the first image. When a similar selection of a laser scanning points close to the tree trunk made from the second image, only those laser points that have actually had a hit on the tree trunk remain. As a result, only small parts of complete laser echoes are selected. Therefore, each sub-part of the superimposed laser echo should include a reference to the original laser echo. The complete laser echoes are illustrated in the last image.
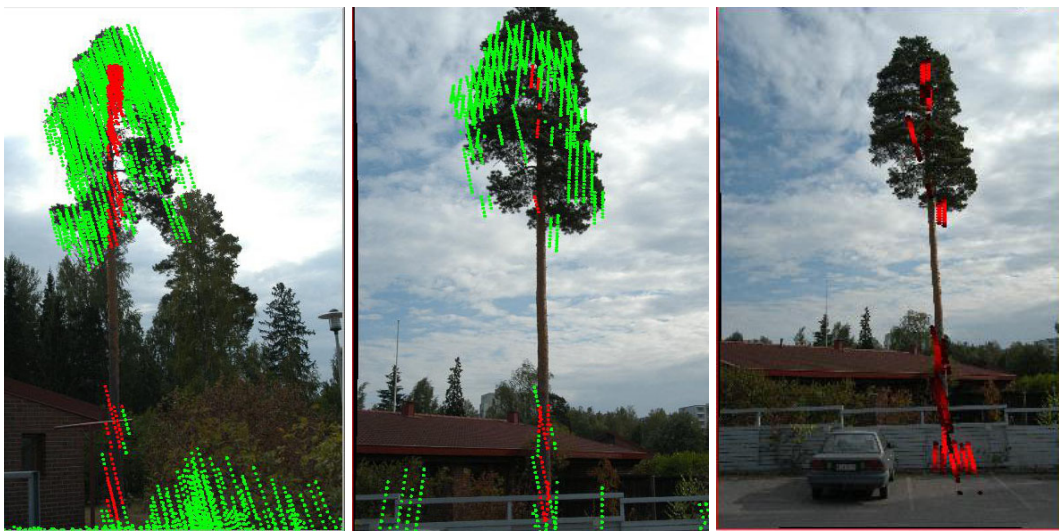
Figure 18. An example, how images can be used for finding the trunk of the tree from the waveform data. The intersection of two perpendicular cross-sections finds potential echoes that have hit the trunk.

After finding all laser echoes that have got a hit from the tree trunk, more detailed examination is possible. In the example studied, such echoes, in which the hit from the tree trunks has not been the first pulse, were examined in more detail. In Figure 19, the laser pulse has first hit the upper canopy of the tree and then returned completely from the tree trunk. Therefore, the last pulse represents the trunk. In the next example (Figure 20), two laser scanning echoes have acted similarly than in the first case, but part of the light ray has passed the tree trunk and continued to the ground. Therefore, the second pulse out of three represents the hit from the tree trunk. In addition, experiment revealed that the pulse from the tree trunk is not as strong as from the ground. One explanation to this phenomenon is that the angle, in which the laser light ray hits surfaces, is different.
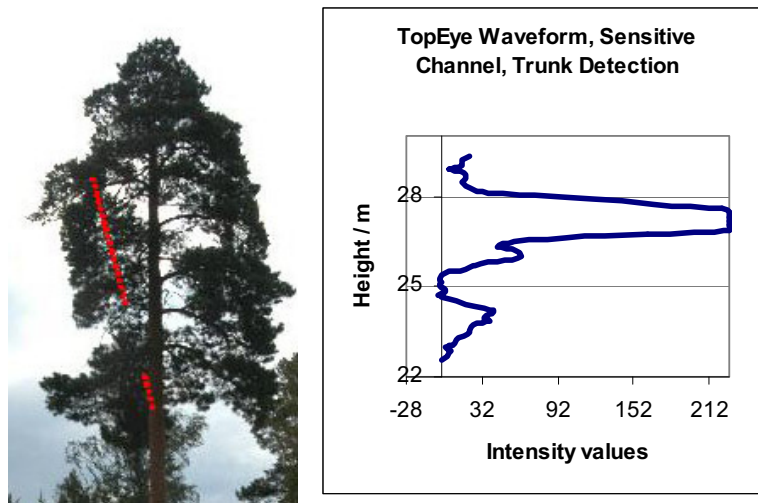
Figure 19. Waveform echo passes through the thick upper foliage before reaching the trunk. The echo is denoted in the image by uniform color in order to enhance the visibility of small intensity values.
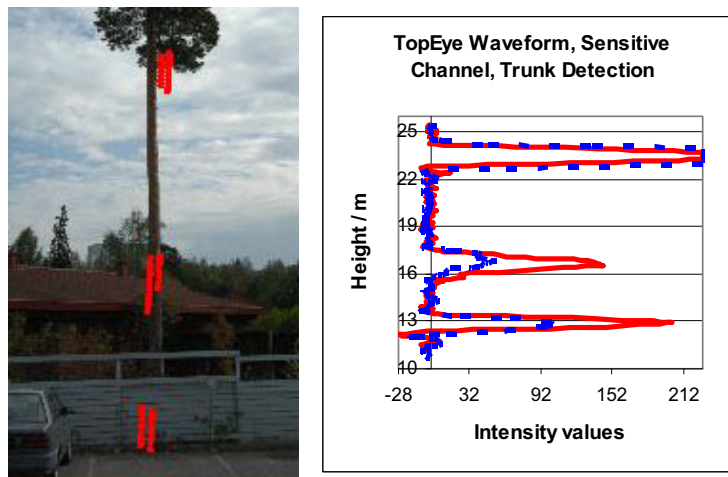
Figure 20. Two similar waveform echoes pass through thin branches of the upper foliage, detecting the trunk and continuing to the ground. The echoes are denoted in the image by uniform color in order to enhance the visibility of small intensity values.

In Paper **VI**, the usability of laser scanning data for measuring heights of lightning poles, walls and fences were investigated. When results from laser scanning data were compared with field surveys, a systematic error of 0.01 m and a standard deviation of 0.15 m were detected. In the case of lightning poles, the behavior of laser scanning was examined more closely by interactively orienting a terrestrial image and the laser point cloud. As can be seen from Figure 21, the point density of both Toposys and TopEye has been enough to detect the upper parts of lightning poles.

Figure 21. Integration of laser point clouds and a terrestrial image illustrates how the point density of both Toposys and TopEye has been sufficient to detect the upper parts of lightning poles. (from Paper **VI**)

5 Discussion

5.1 Applicability and benefits of developed methods

Axelsson (1998) pointed out that in many cases it is impossible to interpret laser data correctly unless oriented image is available. Experiences in this study using interactive orientation have confirmed this statement. Only relatively large features are typically identifiable in the beginning of the orientation process. Using these features, the approximate orientation can be accomplished. When orientation is already close to optimal, small details begin to be understandable. Such details can be, for example, a single hit from a traffic light pole, a fence, an antenna, and a mail box. Even if laser data is quite sparse, small details can typically be detected from laser scanning data. Alone, an individual hit from a single feature is not very informative, but if data includes many of such features, the entity usually fixes the orientation very well. The interactive orientation, unlike other orientation methods, is able to use all these small details as tie features.

From the very beginning, the aim of this thesis was to enable integration of laser scanning data and imagery acquired from the different perspectives. Usually, examples of integration have used data, which has been acquired from approximately the same perspective, as highlighted in Chapter 2.3. Even if for many applications, e.g. for colorizing the laser point cloud, such data is the most feasible, a different perspective gives opportunity for more detailed examination and comparison of data sets, as illustrated in Chapter 4. Only a few publications from other researches can be found that integrates, e.g., airborne laser scanning data and terrestrial images (e.g. Jokinen et al., 2006; Kajuutti et al., 2007). When quite sparse airborne laser scanning data and terrestrial images are oriented together, the difficulty to find tie features automatically is a significant obstacle. Therefore, in many cases interactive methods are only alternatives to finding relative orientations.

Because interactive orientation is based on human interpretation, when laser scanning data is superimposed onto an image using the final orientation, the data usually fits well with the image. As can be seen from the results in Chapter 4.1, this does not mean that orientation is always error-free. However, small rotation errors are compensated for by adjusting camera location in a way that at the image plane the amount of misalignment of superimposed laser scanning data is minimal. For example, in the case of direct orientation sensors, errors of orientation parameters from GPS and IMU typically accumulate, causing significantly larger misalignment of superimposed laser scanning

data, even if the errors of orientation parameters would be at the same level than in the case of interactive orientation.

In addition to solving orientations, superimposing laser data onto images typically reveals, if the internal geometry of laser scanning data is homogeneous. Outliers are easily detectable, when compared against an image. Additionally, the quality of strip-wise orientation can be detected by superimposing overlapping laser scanning areas onto an image. Similarly, the temporal changes between several laser scans and images become visible as illustrated in Figure 12 and Figure 13.

After the orientation, images and laser scanning point clouds can be used together to gain additional information. The final application depends of the type of integration: i.e. object-level integration, photogrammetry aided by laser scanning, laser scanning aided by photogrammetry, or tightly integrated laser scanning and optical images. Only tightly integrated laser scanning and optical images does not require an additional relative orientation after the system calibration.

According to Kern (2001), it is sometimes necessary to attach thematic information, such as physical, chemical, historical or legal properties, to models besides to geometry and textures. Most of thematic information requires a human expert to interpret and attach this information to virtual objects. Geometric information derived from laser scanning data only is not usually enough for retrieving such thematic information. However, the combination of laser scanning data and imagery could significantly aid the interpretation phase.

5.2 Limitations

In some cases, laser scanning data can be too sparse or not enough features are visible on the scene for an accurate orientation, which limits the applicability of the method. Specially, if only terrestrial images are used, the footprint of a single image can be very narrow. Adding more images to the image block is one solution, but imagery should still be acquired in such a way that enough interpretable features are visible. Unfortunately, it is not possible to obtain an optimal set of interpretable features at the image footprints in all cases.

Additionally, the interpretation skills of an operator have influence on the accuracy of orientations. If very sparse laser scanning data or images, whose footprints contain only a few objects, are relatively oriented, the importance of interpretation is particularly emphasized. An experienced operator already knows what kind of features can be expected to be found, while an inexperienced operator requires more time to find such features. On the other hand, if sparse laser scanning data includes a lot of outliers and noise, there might not even be an unambiguous solution. In such case, an operator typically also needs pre-knowledge of the laser scanner instrument and its expected behavior in order to make an optimal decision regarding the best alignment.

In the case of a single image, the opening angle of a lens system may limit the possibility of achieving the most accurate orientation, especially in the forward and backward directions along the optical axes of a camera. Such difficulties derive from the fact that the moving of a camera location along the optical axis causes relatively small changes at the image plane compared with the case in which a camera is moved perpendicular to the optical axis. By replacing a single image with a panoramic image or an image block, geometric difficulties can be overcome as illustrated in Chapters 3.2 and 4.1.

The major disadvantage of the interactive orientation method developed is the lack of automation. Therefore, it may not be feasible to use an interactive orientation individually for a large set of images. Instead, it can be used for solving a relative orientation between large image blocks and adjusted laser scanning strips. In addition, an interactive orientation enables a relative orientation in difficult cases, in which many other orientation strategies would fail. Therefore, it can be seen as an additional method complementing methods giving automatic orientation, especially in cases where automation fails, when higher accuracy is required and when a reasonable small amount of human interaction during the interactive orientation process results in improved accuracy of the larger data set.

Even if an interactive orientation does not provide an automatic solution for solving a relative orientation between laser scanning data and images, in many cases it is a feasible method, especially when the laser scanning point cloud is too sparse or noisy for extracting accurate tie features or the perspective differences prevent the use of such features. The strength of the method is the intelligence of the human operator, who is able to use the entire point cloud as a tie feature as well as to detect even single laser scanning points that have hit an interpretable object and use them all for improving the relative orientation.

Software, which was programmed in order to test the developed methods and algorithms, was not optimized for handling large point clouds during an interactive orientation. Therefore, there is typically a need to reduce the amount of points before an orientation. Usually, it is relatively easy to select laser points from those areas that are the most useful for solving orientations. However, the current implementation limits the full advantage of using complete laser point clouds during the orientation process.

In some cases, the cost of data acquisition may be an obstacle. Optimally, laser scanning data and images are acquired simultaneously. However, for practical reasons this is not always desired. For example, airborne laser scanner can operate also at the night time, which is not possible for the acquisition of photographs. In such case, collecting both data sets requires two flights, which significantly increases costs.

5.3   Future research

No standard procedure exists yet for the orientation of laser scanning data and imagery, even if several researchers have investigated this research question, as was highlighted in Chapter 2.2. In addition, there has been lack for comparison of existing orientation methods. EuroSDR launched a project "Registration Quality – Towards Integration of Laser Scanning and Photogrammetry" in 2009. For this project, a common data set was acquired and delivered to the participant. The focus is to solve relative orientation between DMC aerial images and airborne laser scanning data. It is expected that this project will produce an accurate comparison of several orientation strategy variants. Additionally, the interactive orientation method is included in the project. The plans include completing several interactive orientations of small tie patches along the image block, which will also reveal strip-wise internal errors of laser scanning data. A similar approach was experimented with Rönnholm (2004), but in that paper, the relative orientation was applied only between several overlapping laser scanning point clouds. From one laser data set, a virtual image was created and other laser scanning strips were oriented interactively with it. As a result, the wave-like distortion, depending on the flying direction, was detected along the airborne laser scanning strip indicating that the method has potential for finding internal errors of laser scanning strips caused by inaccurate system calibration of laser scanner.

It is expected that internal errors of laser scanning strips can be detected and corrected more accurately using imagery as a reference. Future research will include experiments on how the interactive orientation is feasible for analyzing the accuracy of laser scanning in large areas. This will require several smaller test patches, in which an interactive orientation is separately performed. Corrections of laser scanner system parameters will be solved using results from test patches.

In addition to new research subjects, the interactive orientation is continued to be used for solving relative orientations of laser scanning data and imagery thus enabling various integration applications that are feasible only after accurate orientations. The software development will continue and the potential for implementing the interactive orientation method in commercial software will also be examined. The method should also be integrated with existing automatic registration methods to be used in cases where full automation does not yield satisfactory results. For example, an interactive orientation could provide a fast approximate orientation. Then, an automatic method could be applied. Visual examination could verify if the automatic orientation has been successful. Finally, if any misalignment between data sets is still visible, the fine tuning could be completed by applying the interactive method again.

Examples within this thesis only include relative orientations of optical images and laser scanning data. Even if this combination is very interesting, it is not the only feasible alternative. For example, Dowman (2004) discussed how airborne laser scanning and interferometric SAR (IfSAR) data could be integrated to create more accurate DEM. The advantage of IfSAR is that it can reach the terrain surface even better than airborne

laser scanning data. In the future, it would be interesting to experiment if the developed interactive orientation method is applicable to the orientation and integration of radar data with laser scanning or images. Furthermore, the future research will include experiments using multi- or hyperspectral images oriented with laser scanning data. It is expected that the integration of these data sets will have a great potential for more advanced classification of, e.g., forestry.

An interactive orientation is feasible also for completing the relative orientation of vector data and images. As mentioned in Paper **II**, an interactive orientation becomes easier if some pre-knowledge about the orientation in known. In some mobile phones, digital compass, GPS, accelerometers and a camera are integrated. Therefore, an approximate orientation for a single image can be achieved. On the other hand, we can make accurate 3D city models in vector format, which can be downloaded to a mobile phone. The interactive orientation could be used for assisting consumers to improve a sensor-based orientation *in situ*. As was highlighted in Ahola et al. (2003), orientation errors are clearly visible when a vector model is superimposed onto an image, and the interactive orientation can be used for correcting initial orientation parameters, which therefore improves positioning accuracy. In addition to navigation, the intuitive orientation tools are also required if consumers begin to participate in map production. One advantage of photogrammetric methods is that cameras are relatively cheap. Therefore, if freeware or shareware photogrammetric software would be available, consumers could produce photorealistic 3D models and add their models in the common platform without significant investments in measuring devices. Currently, the orientation phase is maybe the major obstacle to consumers obtaining an easy access to the ground coordinate system. Therefore, the research of orientation methods is highly relevant. The future vision is that there could be 3D Wikipedia that includes consumer-produced 3D city models and semantic information. Such a system would be a platform for a new kind of interactive social media. The research on the use of the interactive orientation for improving navigation and consumer-based map production will continue within the ongoing project "Economy and technology of a global peer-produced 3D geographical information system in built environment" funded by the Academy of Finland.

6 Conclusions

The integration of laser scanning data and imagery requires that both data sets are in the same coordinate system accurately (Papers **I-VI**). The first objective of the thesis was to develop methods for solving orientations between laser scanning data and digital images or image blocks without limitations in the data acquisition perspective. A method for solving interactively relative orientation between images and laser scanning point clouds was developed (Papers **II** and **III**). The method utilizes tools and strategies for changing location and rotations of images or image blocks and relies on visual matching of superimposed laser data onto images. The method can be used with a single image, but also with stereo or multi-view images.

The results from developed interactive orientations were compared against both ground surveys and the ICP-based registration. The ICP-based registration was calculated between an airborne laser point cloud and a 3D model, which was created mainly using image measurements but also adding some terrestrial laser scanning and geodetic observations. The hypothesis was that by adding more images taken from different perspectives, the accuracy of orientations will increase. The results from experiments within the Otaniemi test area proved that by using image blocks instead of single images, the interpretation errors were decreased, and thus the accuracy of relative orientations increased. In addition, experiments in Paper **III** revealed that if the rotation differences between data sets were known from different sources, the location differences could be found very accurately using an interactive method.

Another hypothesis was that using data from different perspectives was expected to provide a more complete understanding of objects or areas in interest. In the case of the orientation phase, practical experiences (Papers **II**-**VI**) confirmed that the interpretation of corresponding features is easier, and the orientation accuracy better, if more than one image is used.

In the case of data integration, several examples in Papers **I-VI** illustrated how images provide geometrical and radiometric information that is additional to laser scanning data, and which can be used, e.g., for verification of the internal accuracy of laser scanning data, for supporting classification of laser scanning data, for detecting temporal changes, for examining the interaction of laser scanning data with objects, and for enhancing laser points clouds with natural or false colors.

Another hypothesis was that the different viewing perspectives of data sources reveal the behavior of laser scanning data. The behavior of both first echoes and full waveforms of laser scanning were successfully examined using imagery as a reference

(Papers **I-VI**). Examples were presented from urban environments and forestry. As was expected, images appeared to be well-suited for examination of details of laser data enabling advanced interpretation, change detection and outlier identification.

The last sub-goal was to experience data fusion by colorizing laser point clouds from images that were acquired from very different perspectives, such as terrestrial and airborne images. In Paper **III**, an example was illustrated in which airborne laser scanning data and terrestrial laser scanning data were integrated and colorized using both aerial and terrestrial imagery. This example highlighted how integrating multi-source and multi-angle data enables more complete photorealistic 3D modeling.

In the future, integrated and orientated multi-source and multi-angle data will, most probably, be the major data source for mapping and 3D modeling. Therefore, the research on these subjects should be continued in order to improve existing methods and to develop accurate, flexible and efficient methods and processes.

7 References

Abdelhafiz A., Riedel, B., and Niemeier, W., 2005. 3D image approach as a result from the combination between the laser-scanner point cloud and the digital photogrammetry. In: Grün/Kahmen (eds), Optical 3-D Measurement Techniques VII, Vol I, pp. 204-213.

Abmayr, T., Dalton, G., Hätrl, F., Hines, D., Liu, R., Hirzinger, G., and Frölich, C., 2005. Standardization and visualization of 2.5D scanning data and color information by inverse mapping. In: Grün/Kahmen (Eds.), Optical 3-D Measurement Techniques VII, Vol. I, pp. 164-173.

Ahola, J., Kortekangas, A., Kummala, J., Kylänpää, M., Laakko, T., Lehto, L. Lehtonen, M., Leppinen, T., Leppänen, J., Lähteenmäki, J., Martamo, R., Ruotsalainen, R., Rönnholm, P., Toivonen, S., Törönen, J., and Vermeer, M., 2003. Service architecture and metadata (PAM). Deliverable PAM-6. Personal navigation service architecture: survey of background and standards. VTT Industrial Systems, Espoo, 79 pages.

Al-Manasir, K. and Fraser, C., 2006. Registration of terrestrial laser scanner data using imagery. The Photogrammetric Record, 21(115), pp. 255-268.

Aldred, A. and Bonnor, G., 1985. Application of airborne lasers to forest surveys. Information Report PI-X-51, Canadian Forestry Service, Petawawa National Forestry Institute, 62 p.

Alshawabkeh Y. and Haala N., 2004. Integration of digital photogrammetry and laser scanning for heritage documentation. International Archives of Photogrammetry, Remote Sensing and Spatial Information Sciences, 35(Part B5), pp. 424-429.

Axelsson, P., 1998. Integrated sensors for platform orientation and topographic data acquisition. Proceedings of the Symposium on Digital Photogrammetry, May 21-22, Istanbul, Turkey, pp. 1-11. http://www.adelaide.se/topeye/istanb~2.pdf (Accessed September 9, 2009)

Baltsavias, E., 1999. A comparison between photogrammetry and laser scanning. ISPRS Journal of Photogrammetry and Remote Sensing, 54(2∕3), pp. 83–94.

Besl, P. and Jain, R., 1988. Segmentation through variable-order surface fitting. IEEE Transactions on Pattern Analysis and Machine Intelligence, 10(2), pp. 167-192.

Bilker, M. and Kaartinen, H., 2001. The quality of real-time kinematic (RTK) GPS positioning. Reports of the Finnish Geodetic Institute 2001:1, Kirkkonummi, 25 pages.

Blais, F., Beraldin, J.-A., El-Hakim, S., and Godin, G., 2003. New development in 3D laser scanners: from static to dynamic multi-modal systems. Proceeding of the 6th Conference on Optical 3-D Measurement Techniques (3DIM), September 22-25, Zurich, Switzerland, 8 pages. http://www.prip.tuwien.ac.at/cvch07/download/ download/lectures/NRC-45884.pdf (Accessed October 17, 2009)

Blais, F., 2004. Review of 20 years of range sensor development. Journal of Electronic Imaging, 13(1), pp. 231-240.

Brown, D., 1971. Close-range camera calibration. Photogrammetric Engineering and Remote Sensing, 37(8), pp.855-866.

Burman, H., 2002. Laser strip adjustment for data calibration and verification. International Archives of Photogrammetry and Remote Sensing, 34(3), pp. 67–72.

Böhm, J. and Haala, N., 2005. Efficient integration of aerial and terrestrial laser data for virtual city modeling using lasermaps. International Archives of Photogrammetry and Remote Sensing, 36(Part 3/W19), pp. 192–197.

Cramer, M., 2009. Digital camera calibration. EuroSDR Official Publication No 55, 257 pages.

Crombaghs, M., Brügelmann, R., and De Min, E., 2000. On the adjustment of overlapping strips of laseraltimeter height data. International Archives of Photogrammetry and Remote Sensing, 33(Part B3), pp. 230–237.

Csanyi, N. and Toth, C., 2007. Improvement of lidar data accuracy using lidar-specific ground targets. Photogrammetric Engineering & Remote Sensing, 73(4), pp. 385–396.

Deng, F., Zhang, Z., and Zhang, J., 2004. Construction 3D urban model from lidar and image sequence. International Archives of Photogrammetry and Remote Sensing and Spatial Information Sciences, 35 (Part 3), pp. 580-583.

Dias, P., Sequeira, V., Gonçalves, J., and Vaz, F., 2002. Automatic registration of laser reflectance and colour intensity images for 3D reconstruction. Robotics and Autonomous Systems, 39, pp. 157-168.

Dold, C. and Brenner, C., 2006. Registration of terrestrial laser scanning data using planar patches and image data. International Archives of the Photogrammetry, Remote Sensing and Spatial Information Sciences 36 (Part 5), pp. 25–27.

Dowman, I., 2004. Integration of lidar and IfSAR for mapping, International Archives of Photogrammetry and Remote Sensing and Spatial Information Sciences, 35(Part B2), pp. 90-100.

El-Hakim, S. and Beraldin, J.-A., 1994. On the integration of range and intensity data to improve vision-based three-dimensional measurements. Videometrics III, SPIE, 2350, pp. 306-321.

El-Hakim, S., Whiting, E., Gonzo, L., and Girardi, S., 2005. 3-D reconstruction of complex architectures from multiple data. 3D Virtual Reconstruction and Visualization of Complex Architectures (3D-Arch'2005), August 22-24, Venice-Mestre, Italy, 8 pages. http://www.3dphotomodeling.org/3d-arch-05.pdf (accessed September 25)

El-Sheimy, N., 2005. An overview of mobile mapping systems. FIG Working Week 2005 and GSDI-8, From Pharaohs to Geoinformatics, 16-21 April, Cairo, Egypt, 24

pages. http://www.fig.net/pub/cairo/papers/ts_17/ts17_03_elsheimy.pdf (accessed September 25)

Filin, S., 2003. Recovery of systematic biases in laser altimetry data using natural surfaces. Photogrammetric Engineering & Remote Sensing, 69(11), pp. 1235–1242.

Forkuo, E. and King, B., 2004. Automatic fusion of photogrammetric imagery and laser scanner point clouds. International Archives of Photogrammetry, Remote Sensing and Spatial Information Sciences, 35 (Part B4), pp. 921–926.

Fraser, C., 1989. Optimization of networks in non-topographic photogrammetry. In Karara, H. (Editor) Non-Topographic Photogrammetry, Second edition, ASPRS, Virginia, USA, ISBN 0-944426-10-7, pp. 95-106.

Fraser, C., 1992. Photogrammetric measurement to one part in a million. Photogrammetric Engineering & Remote Sensing, 58(3), pp. 305-310.

Fraser, C. and Hanley, H., 2004. Developments in close range photogrammetry for 3D modelling: the iWitness example. Proceedings of International Workshop on Processing & Visualization Using High-Resolution Imagery, Pitsanulok, Thailand, 4 pages. http://www.photogrammetry.ethz.ch/pitsanulok_workshop/ papers/09.pdf (accessed April 16, 2009).

Gaveau, D. and Hill, R., 2003. Quantifying canopy height underestimation by laser pulse penetration in small-footprint airborne laser scanner data. Canadian Journal of Remote Sensing 29, pp. 650-657.

Gomes Pereira, L. and Janssen, J., 1999. Suitability of laser data for DTM generation: case study in the context of road planning and design. ISPRS Journal of Photogrammetry & Remote Sensing, 54, pp. 244-253.

Gruber, D., 2000. The mathematics of the 3D rotation matrix. Presented at the Xtreme Game Developers Conference, September 30-October 1, Santa Clara, California, http://www.fastgraph.com/makegames/3drotation/ (accessed August 9, 2009).

Guarnier, A., Remondino, F., and Vettore, A., 2006. Digital photogrammetry and TLS data fusion applied to cultural heritage 3D modeling. International Archives of the Photogrammetry, Remote Sensing and Spatial Information Sciences, 36, 6 pages. http://www.photogrammetry.ethz.ch/general/persons/fabio/Guarnieri_etal_ISPRSV 06.pdf (accessed September 25)

Haala, N. and Anders, K.-H., 1997. Acquisition of 3D urban models by analysis of aerial images, digital surface models and existing 2D building informatton. SPIE Conference on Integrating Photogrammetnc Techniques with Scene Analysis and Machme Vision III, SPIE Proceedings, 3072, pp. 212-222.

Haala, N., Brenner, C., and Stätter, C., 1998. An integrated system for urban model generation, International Archives of Photogrammetry and Remote Sensing, 36(Part 2), pp. 96-103.

Habib, A., Ghanma, M., Morgan, M., and Mitishita, E., 2004. Integration of laser and photogrammetric data for calibration purposes. International Archives of the

Photogrammetry, Remote Sensing and Spatial Information Sciences. 35 (Part B2) pp. 170-175.

Habib, A., Ghanma, M., Morgan, M., and Al-Ruzouq, R., 2005. Photogrammetric and lidar data registration using linear features. Photogrammetric Engineering & Remote Sensing, 71(6), pp. 699-707.

Haggrén, H., Manninen, T., Peräläinen, I., Pesonen, J., Pöntinen, P., and Rantasuo, M., 1995. Airborne 3D profilometer. SPIE Proceedings, 2646, pp. 202-211.

Haggrén, H., Pöntinen, P., and Mononen, J., 1998. Cocentric image capture for photogrammetric triangulation and mapping and for panoramic visualization. IS&T/SPIE's 11th Annual Symposium on Electronic Imaging: Science and Technology, 23 to 29 January 1999, San Jose, California USA, SPIE Proceedings, 3641, pp. 17-21.

Hara, K., Kabashima, Y., Iwashita, Y., Kurazume, R., and Hasegawa, T., 2007. Robust 2D-3D alignment based on geometrical consistency. Proceeding of Sixth IEEE International conference on 3-D Digital Imaging and Modelling (3DIM), Montreal, Canada, pp. 273–280.

Heipke, C., Jacobsen K., and Wegmann H., 2002. Analysis of the results of the OEEPE test Integrated Sensor Orientation. Test Report and Workshop Proceedings, OEEPE Official Publication n. 43, pp. 31–45.

Honkavaara, E., Ilves, R., and Jaakkola, J., 2003. Practical results of GPS/IMU/camera-system calibration. Proceedings of International Workshop: Theory, Technology and Realities of Inertial/GPS Sensor Orientation, Castelldefels, Spain, 10 pages. http://www.isprs.org/commission1/theory_tech_realities/pdf/p06_s3.pdf (accessed September 29, 2009)

Hulme, K., Collins B., Constant G., Pinson J., 1981. A CO2 laser rangefinder using heterodyne detection and chirp pulse compression. Optical and Quantum Electronics, 13, pp. 35-45.

Hyyppä, J. and Inkinen, M., 1999. Detecting and estimating attributes for single trees using laser scanner. The Photogrammetric Journal of Finland, 16(2), pp. 27-42.

Hyyppä, J., Hyyppä, H., Litkey, P., Yu, X., Haggren, H., Rönnholm, P., Pyysalo, U., Pitkaenen, J., and Maltamo, M., 2004. Algorithms and methods of airborne laser-scanning for forest measurements. International Archives of the Photogrammetry, Remote Sensing and Spatial Information Sciences, 36(Part 8/W2), pp. 82-89.

Hyyppä, J., Hyyppä, H., Leckie, D., Gougeon, F., Yu, X., and Maltamo, M., 2008. Review of methods of small-footprint airborne laser scanning for extracting forest inventory data in boreal forests. International Journal of Remote Sensing, 29(5), pp. 1339-1366.

Jaakkola, A., Hyyppä, J., Kukko, A., Yu, X., Lin, Y., Kaartinen, H., and Lehtomäki, M., 2010. A low-cost multi-sensoral vehicle-based mobile mapping system. International Journal of Photogrammetry and Remote Sensing, ISPRS 100 years special issue. Submitted.

Jarvis, R., 1983. A laser time-of-flight range scanner for robotic vision. IEEE Transactions on pattern analysis and Machine Intelligence, Vol. PAMI-5, No. 5, pp. 505-512.

Jokinen, O., Pyysalo, U., and Pöntinen, P., 2006. Determination of corresponding trunks in a pair of terrestrial images and airborne laser scanner data. The Photogrammetric Journal of Finland, 20(1), pp. 35-44.

Kaasalainen, S., Lindroos, T., and Hyyppä, J., 2007. Toward hyperspectral lidar: measurement of spectral backscatter intensity with a supercontinuum laser source. IEEE Geoscience and Remote Sensing Letters, 4(2), pp. 211-215.

Kager, H., 2004. Discrepancies between overlapping laser scanning strips - simultaneous fitting of aerial laser scanner strips. International Archives of Photogrammetry and Remote Sensing and Spatial Information Sciences, 35(Part B/1), pp. 555–560.

Kahlmann, T. and Ingensand, H., 2005. Calibration and improvements of the high-resolution range-imaging camera SwissRanger^{TM}. Videometrics VIII, SPIE Proceedings, 5665, pp. 144-155.

Kajuutti, K., Jokinen, O., Geist, T., and Pitkänen, T., 2007. Terrestrial photography for verification of airborne laser scanner data on Hintereisferner in Austria. Nordic Journal of Surveying and Real Estate Research, 4, pp. 24–39.

Kamgar-Parsi, B., 2003. Algorithms for matching 3D line sets. IEEE Transactions on Pattern Analysis and Machine Intelligence, 26(5), pp. 582-593.

Kern, F., 2001. Supplementing laserscanner geometric data with photogrammetric images for modeling. The CIPA International Archives for Documentation of Cultural Heritage, Vol. XVIII, 18-21 Sept., Postdam, Germany, pp. 454- 461.

Kilian, J., Haala, N., and Englich, M., 1996. Capture and evaluation of airborne laser scanner data. International Archives of Photogrammetry and Remote Sensing, 31 (Part B3), pp. 383–388.

Konecny, G., 1985. The International Society for Photogrammetry and Remote Sensing – 75 years old, or 75 years young. Photogrammetric Engineering & Remote Sensing, 51(7), pp. 919-933.

Kornus, W. and Ruiz, A., 2003. Strip adjustment of LiDAR data. International Archives of Photogrammetry and Remote Sensing. 34(3), pp. 47–50.

Koschan, A., 1993. A framework for area-based and feature-based stereo vision. Machine Graphics & Vision, 2(4), pp. 285-308.

Kraus, K. and Pfeifer, N., 2001. Advanced DTM generation from LIDAR data. International Archives of Photogrammetry and Remote Sensing, 34(3/W4), pp. 23–30.

Kremer, J., 2001. CCNS and AEROcontrol: Products for efficient photogrammetric data collection. In Fritsch/Spiller (eds.), Photogrammetric Week 2001, Wichmann Verlag, Heidelberg, Germany, pp. 85–92.

Kukko, A., 2001. Digitaalikameran asemointi pallopanoraamajalustaan (Panoramic Rotation Platform for Mounting of Digital Camera. The Institute of Photogrammetry and Remote Sensing, Helsinki University of Technology, Espoo. 20 pages. (in Finnish)

Kukko, A., Andrei, C.-O., Salminen, V.-M., Kaartinen, H., Chen, Y., Ronnholm, P., Hyyppä, H., Hyyppä, J., Chen, R., Haggren, H., Kosonen, I., and Capek, K., 2007. Road environment mapping system of the Finnish Geodetic Institute - FGI ROAMER. International Archives of Photogrammetry, Remote Sensing and Spatial Information Sciences, 36(3/W52), pp. 241-247.

Kurazume, R., Nishino, K., Zhang, Z, and Ikeuchi, K., 2002. Simultaneous 2D images and 3D geometric model registration for texture mapping utilizing reflectance attribute. Proceedings of the 5th Asian Conference on Computer Vision, 23-25 January, Melbourne, Australia, Vol. I, pp. 99-106.

Lange, R. and Seitz, P., 2000. Seeing distances – a fast time-of-flight 3D camera. Sensor Review, 20(3), pp. 212-217.

LaRocque, P. and West, G., 1999. Airborne Laser Hydrography: an introduction. Proceedings of ROPME/PERSGA/IHB Workshop on Hydrographic Activities in the ROPME Sea area and Red Sea, October 24-27, Kuwait, 16 pages. http://www.jalbtcx.org/downloads/Publications/28LaRoque_West_99.pdf (accessed October 24, 2009)

Leckie, D., Gougeon, F., Hill, D., Quinn, R., Armstrong, L., and Shreenan, R., 2003. Combined high-density lidar and multispectral imagery for individual tree crown analysis. Canadian Journal of Remote Sensing 29, pp. 633-649.

Lee, I. and Choi, Y., 2004. Fusion of terrestrial laser scanner data and images for building reconstruction. International Archives of Photogrammetry and Remote Sensing and Spatial Information Sciences, 35(Part B5), pp. 1049-1054.

Lemmens, M., 2007a. Airborne lidar sensors. GIM International, 21(2), 4 pages. http://www.gim-international.com/files/productsurvey_v_pdfdocument_11.pdf (accessed October 24, 2009)

Lemmens, M., 2007b. Product survey on DPW. GIM International, 21(12), 4 pages. http://www.gim-international.com/files/productsurvey_v_pdfdocument_23.pdf (accessed August 12, 2009)

Lemmens, M., 2009. Terrestrial laser scanners. GIM International, 23(8), pp. 62-67. http://www.gim-international.com/files/productsurvey_v_pdfdocument_33.pdf (accessed February 10,2010)

Lichti, D. and Licht, G., 2006. Experiences with terrestrial laser scanner modelling and accuracy assessment. International Archives of Photogrammetry and Remote Sensing and Spatial Information Sciences, 36(Part B5), pp. 155–160.

Lichti, D., 2008. Self-calibration of a 3D range camera. International Archives of the Photogrammetry, Remote Sensing and Spatial Information Sciences, 36(B5), pp. 927-932.

Liu, W., Qu, Y., Wang, C., and Yu, W., 2004. A hybrid stereo matching algorithm using wavelet modulus maxima based on feature and area process. Proceedings of the 2004 IEEE International Conference on Robotics and Biomimetics August 22 - 26, 2004, Shenyang, China, pp. 569-573.

Luhmann, T., 2004. A historical review on panorama imagery. International Archives of Photogrammetry and Remote Sensing, 34(5/W16), 8 pages.

Luzum, B., Starek, M., and Slatton, K., 2004. Normalizing ALSM intensities. Geosensing Engineering and Mapping (GEM) Center Report No. Rep_2004_07_001, Civil and Coastal Engineering Department, University of Florida, 8 pages. http://www.aspl.ece.ufl.edu/reports/GEM_Rep_2004_07_001.pdf (accessed September 25, 2009)

McIntosh, K., Krupnik, A., and Schenk, T., 1999. Utilizing airborne laser altimetry for the improvement of automatically generated DEMs over urban areas. International Archives of Photogrammetry and Remote Sensing, 32(Part B3), pp. 563-569.

Menci, L. and Rinaudo, F., 2007. New trends in digital photogrammetry teaching and diffusion: the Z-Glif software. XXI International CIPA Symposium, 01-06 October, Athens, Greece, 4 pages. http://cipa.icomos.org/fileadmin/papers/ Athens2007/ FP097.pdf (accessed August 12, 2009)

Mitishita, E., Habib, A., Centeno, J., Machado, A., Lay, J., and Wong, C., 2008. Photogrammetric and lidar data integration using the centroid of a rectangular roof as a control point. Photogrammetric Record, 23(121), pp. 19–35.

Morris, J., Porter, D., Neet, M., Noble, P., Schmidt, L., Lapine, L., and Jensen, J., 2005. Integrating LIDAR elevation data, multi-spectral imagery and neural network modelling for marsh characterization. International Journal of Remote Sensing, 26(23), pp. 5221-5234.

Oggier, T., Lehmann, M., Kaufmann, R., Schweizer, M., Richter, M., Metzler, P., Lang, G., Lustenberger, F., and Blanc, N., 2004. An all-solid-state optical range camera for 3D-real-time imaging with sub-centimeter depth-resolution (SwissRanger^{TM}). Proc. SPIE Vol. 5249, pp. 634-545.

Paar, G., Bauer, A., and Kontrus, H., 2005. Texture based fusion between laser scanner and camera for tunnel surface documentation. In Grün/Kahmen (Eds.): Optical 3-D Measurement Techniques VII, Vol. 1, pp. 74-80.

Park, S.-Y. and Baek, J., 2007. Online registration of multi-view range images using geometric and photometric feature tracking. Proceedings of IEEE International Conference on 3-D Digital Imaging and Modeling (3DIM07), Montréal, Canada, August 21-23, pp. 281-288.

Persson, Å., Holmgren, J., and Söderman, U., 2002. Detecting and measuring individual trees using an airborne laser scanner. Photogrammetric Engineering & Remote Sensing 68, pp. 925-932.

Persson, Å., Holmgren, J., Södermann, U., and Olsson, H., 2004. Tree species classification of individual trees in Sweden by combining high resolution laser data

with high resolution near-infrared digital images. Proceedings of the ISPRS Working Group VIII/2 Laser-Scanners for Forest and Landscape Assessment, pp. 204-207.

Persson, Å., Söderman, U., Töpel, J., and Ahlberg, S., 2005. Visualization and analysis of full-waveform airborne laser scanner data. International Archives of Photogrammetry, Remote Sensing and Spatial Information Sciences, 36, pp. 103–108.

Pesci, A. and Teza, G., 2008. Terrestrial laser scanner and retro-reflective targets: An experiment for anomalous effects investigation. International Journal of Remote Sensing, 29, pp. 5749–5765.

Pfeifer, N., 2005. Airborne laser scanning strip adjustment and automation of tie surface measurement. Boletim de Ciências Geodésicas, 11(1), Curitiba, Brasil, pp. 3-23.

Pfeifer, N. and Briese, C., 2007. Geometrical aspects of airborne laser scanning and terrestrial laser scanning. International Archives of Photogrammetry, Remote Sensing and Spatial Information Sciences, 36(3/W52), pp. 311-319.

Postolov, Y., Krupnik, A., and McIntosh, K., 1999. Registration of airborne laser data to surfaces generated by Photogrammetric means. International Archives of Photogrammetry and Remote Sensing, 32(Part 3/W14), pp. 95-99.

Przybilla, H., 2006. Fusion of terrestrial laser scanning and digital photogrammetry. International Archives of Photogrammetry, Remote Sensing and Spatial Information Sciences, 36 (Part 5), 5 pages. http://www.isprs.org/commission5/proceedings06/paper/1235_Dresden06.pdf (accessed September 25)

Pöntinen, P., 2000. On the creation of panoramic images from image sequences. International Archives of Photogrammetry and Remote Sensing, 33(Part B5/2), pp. 635-641.

Ray, L., Gabello, L., and Repich, K, 2001. Approaches to a color scannerless range imaging system. 3rd International Conference on 3D Digital Imaging and Modeling (3DIM 2001), Quebec City, Canada, pp. 20-27.

Ressl, C., Haring A., Briese, C., and Rottensteiner, F., 2006. A concept for adaptive mono-plotting using images and laserscanner data. International Archives for Photogrammetry and Remote Sensing, 36(3), pp. 98-104.

Rocchini, C., Cignomi, P., Montani, C., and Scopigno, R., 1999. Multiple textures stitching and blending on 3D objects. Proceedings of 10th Eurographics Workshop on Rendering, Granada, Spain, pp. 119-130.

Rottensteiner, F., Trinder, J., Clode, S., Kubik, K., and Lovell, B., 2004. Building detection by Dempster-Shafer Fusion of LIDAR data and multispectral aerial imagery. Proceedings of the 17th International Conference on Pattern Recognition (ICPR'04), Cambridge, United Kingdom, pp. 339-342.

Rottensteiner, F., Trinder, J., Clode, S., and Kubik, K., 2007. Building detection by fusion of airborne laser scanner data and multi-spectral images: Performance

evaluation and sensitivity analysis. ISPRS Journal of Photogrammetry & Remote Sensing, 62, pp. 135-149.

Roux, M., 2004. Registration of airborne laser data with one aerial image. International Archives of the Photogrammetry, Remote Sensing and Spatial Information Sciences, 35 (Part B3), pp. 1043-1048.

Rönnholm, P., 2004. The evaluation of the internal quality of laser scanning strips using the interactive orientation method and point clouds. International Archives of the Photogrammetry, Remote Sensing and Spatial Information Sciences, 35 (Part B3), pp. 255-261.

Rönnholm, P., Pöntinen, P., Nuikka, M., Suominen, A., Hyyppä, H., Kaartinen, H., Absetz, I., Hirsi, H., and Hyyppä, J., 2006. Experiments on deformation measurements of "Helsinki Design Week 2005" info pavilion. International Archives of the Photogrammetry, Remote Sensing and Spatial Information Sciences, 36(Part 5), pp. 273-278.

Salemi, G., Achilli, V., and Cervato, C., 2005. Data acquisition for cultural heritage navigation: Integration of panoramic imaging, terrestrial laser scanning and anaglyphs. International Archives of Photogrammetry, Remote Sensing and Spatial Information Sciences, 36(5/W8), pp. 1-6.

Scheibe, K., Scheele, M., and Klette, R., 2004, Data fusion and visualization of panoramic images and laser scans. International Archives of Photogrammetry, Remote Sensing and Spatial Information Sciences, 34(Part 5/W16), 8 pages. http://www.commission5.isprs.org/wg1/workshop_pano/papers/ PanoWS_Dresden2004_Scheibe.pdf (accessed October 5, 2009)

Schenk, T., 2001. Modeling and analyzing systematic errors in airborne laser scanners. Technical Notes in Photogrammetry No 19, The Ohio State University, Columbus, USA, 46 pages.

Schenk, T., Seo, S., and Csatho, B., 2001. Accuracy study of airborne laser scanning data with photogrammetry. International Archives of the Photogrammetry, Remote Sensing and Spatial Information Sciences, 34(3/W4), pp. 113-118.

Schenk, T. and Csathó, B., 2002. Fusion of LIDAR data and aerial imagery for a more complete surface description. International Archives of the Photogrammetry, Remote Sensing and Spatial Information Sciences, 34 (3), pp. 310–317.

Schenk, T., 2004. From point-based to feature-based aerial triangulation. ISPRS Journal of Photogrammetry &Remote Sensing, 58, pp. 315-329.

Schiewe, J., 2003. Integration of multi-sensor data for landscape modeling using a region-based approach. ISPRS Journal of Photogrammetry & Remote Sensing, 57, pp. 371-379.

Schnadt, K. and Katzenbeisser, R., 2004. Unique airborne fiber scanner technique for application-oriented lidar products. International Archives of Photogrammetry, Remote Sensing and Spatial Information Sciences, 36(8/W2), pp. 19-23.

Schroeder, W., Forgber, E., and Estable, S., 1999. Scannerless laser range camera, Sensor Review, 19(4), pp. 285-291.

Silveira, M., Feitosa, R., Jacobsen, K., Brito, J., and Heckel, Y., 2008. A hybrid method for stereo image matching. International Archives of Photogrammetry, Remote Sensing and Spatial Information Sciences, 37(B1), pp. 895-900.

Smith, P. and Elstrom, M., 1999. Automatic feature correspondence for scene reconstruction. Proceedings of the Second International Conference on 3-D Digital Imaging and Modeling (3DIM99), Ottawa, Ont., Canada, October 4-8, pp. 463-472.

Sohn, G. and Dowman, I., 2007. Data fusion of high-resolution satellite imagery and LiDAR data for automatic building extraction. ISPRS Journal of Photogrammetry & Remote Sensing, 62, pp. 43-63.

Stamos, I. and Allen, P., 2000. 3-D model construction using range and image data. Conference on Computer Vision and Pattern Recognition (CVPR 2000), 13-15 June, Hilton Head, SC, USA, pp. 531-536.

Tournas L. and Tsakiri, M., 2005. Point cloud registration using orthophotos. In Grün/Kahmen (Eds.): Optical 3-D Measurement Techniques VII, Vol. 1, pp. 187-193.

Tarrant, J., 2007. Understanding digital cameras: Getting the best image from capture to output. Focal Press, 360 pages, ISBN: 0-240-52024-6.

Toth, C. and Grejner-Brzezinska, D., 2005. Traffic flow estimation from airborne imaging sensors: a performance analysis. ISPRS Workshop "High-Resolution Earth Imaging for Geospatial Information", 17-20 May, Hannover, Germany, 7 pages. http://www.ipi.uni-hannover.de/fileadmin/institut/pdf/141-toth.pdf (accessed September 9, 2009)

Toth, C., Paska, E., and Brzezinska, D., 2007. Using pavement markings to support the QA/QC of lidar data. International Archives of Photogrammetry, Remote Sensing and Spatial Information Sciences, 36 (Part 3/W49B), pp. 173–178.

Triggs, B., McLauchalan, P., Hartley, R., and Fitzgibbon, F., 1999. Bundle adjustment – a modern synthesis. In Triggs, B, Zisserman, A., Szeliski, R (Eds.). Proceedings of the International Workshop: Vision Algorithms'99, Corfu, Greece, pp. 298-372.

Ullrich, A., Reichert, R., Schwarz, R., and Riegl, J., 2001. Time-of-flight-based 3D imaging sensor with true-color channel for automated texturing. In Grün/Kahmen (Eds.): Optical 3-D Measurement Techniques V, Vienna, Austria, pp. 2-9.

Ullrich, A., Schwarz, R., and Kager, H., 2003. Using hybrid multi-station adjustment for an integrated camera laser-scanner system. In Grün/Kahmen (Eds.): Optical 3-D Measurement Techniques VI, Zurich, Switzerland, pp. 298-305.

Umeda, K., Godin, G., and Rioux, M., 2004. Registration of range and color images using gradient constraints and range intensity images. Proceedings of the 17th Conference on Pattern Recognition (ICPR'04), pp. 12–15.

Vosselman, G. and Maas, H.-G., 2001. Adjustment and filtering of raw laser altimetry data. Proceedings of OEEPEWorkshop on Airborne Laserscanning and Interferometric SAR for Detailed Digital Terrain Models, Stockholm, Sweden, 11 pages. http://www.tu-dresden.de/ipf/photo/publikationen/aeltere/ Vosselmann_Maas_OEEPEStockholm2001.pdf (Accessed September 25, 2009)

Vosselman, G., 2008. Analysis of planimetric accuracy of airborne laser scanning surveys. International Archives of Photogrammetry, Remote Sensing and Spatial Information Sciences, 37(Part 3A), pp. 99-104.

Wagner, W., Ullrich, A., Ducic, V., Melzer, T., and Studnicka, N., 2006. Gaussian decomposition and calibration of a novel small-footprint full-waveform digitizing airborne laser scanner. ISPRS Journal of Photogrammetry and Remote Sensing, 60, pp. 100–112.

Wagner, W., Hollaus, M., Briese, C., and Ducic, V., 2008. 3D vegetation mapping using small-footprint full-waveform airborne laser scanners. International Journal of Remote Sensing, 29(5), pp. 1433–1452.

Wang, C., Menenti, M., Stoll, M.-P., Feola, A., Belluco, E., and Marani, M., 2009. Separation of Ground and Low Vegetation Signatures in LiDAR Measurements of Salt-Marsh Environments. IEEE Transactions on Geoscience and Remote Sensing, 47(7), pp. 2014-2023.

Wehr, A. and Lohr, U., 1999. Airborne laser scanning – an introduction and overview. ISPRS Journal of Photogrammetry & Remote Sensing, 54, pp. 68–82.

Wehr, A. and Wiedermann, A., 1999. Fusion of photogrammetric and laser scanner data. XVII CIPA International Symposium, October 3-6, Olinda, Brasil, 5 pages. http://cipa.icomos.org/fileadmin/papers/olinda/99c408.pdf (accessed September 7, 2009)

Wendt, A. and Dold, C., 2005. Estimation of interior orientation and eccentricity parameters of a hybrid imaging and laser scanning sensor. International Archives of Photogrammetry, Remote Sensing and Spatial Information Sciences, 36 (5/W8), 5 pages. http://www2.informatik.hu-berlin.de/~knauer/ISPRS/ panoramicworkshop2005/Paper/PanoWS_Berlin2005_Wendt.pdf (Accessed September 29, 2009)

Wendt and Heipke, 2006. Simultaneous orientation of brightness, range and intensity images. International Archives of Photogrammetry, Remote Sensing and Spatial Information Sciences, 36(Part 5), pp. 315-322.

Wendt, A., 2007. A concept for feature based data registration by simultaneous consideration of laser scanning data and photogrammetric images. ISPRS Journal of Photogrammetry & Remote Sensing, 62, pp. 122-134.

Wiedemann, A., Moré, J., Suthau, T., Theodoropoulou, I., Weferling, U., and Ergün, B., 2001. Comparison of bundle block adjustments for close range applications. In: O. Altan & L. Gründig (eds.) Fourth Turkish-German Joint Geodetic Days. Berlin, Germany, April 2-6, Vol. I, pp. 211-218. http://srv-43-200.bv.tu-berlin.de/ publications/pdf/wiedemann01_bundle.pdf (accessed August 9, 2009)

Yastikli, N., Toth, C., and Brzezinska, D., 2008. Multi sensor airborne systems: The potential for in situ sensor calibration. International Archives of Photogrammetry, Remote Sensing and Spatial Information Sciences, 37(Part B1/I), pp. 89-94.

Yu, X., Hyyppä, J., Kaartinen, H., and Maltamo, M., 2004. Automatic detection of harvested trees and determination of forest growth using airborne laser scanning. Remote Sensing of Environment 90, pp. 451-462.

Zhao, W., Nister, D., and Hsu, S., 2005. Alignment of continuous video onto 3D point cloud. CVPR, 2, pp. 964-971.

Zhang, A., Hu, S., Jin, X., and Sun, W., 2005a. A method merging aerial images and ground laser. Geoscience and Remote Sensing Symposium (IGARSS'05), Vol. I, pp. 222-225.

Zhang, Y., Zhang, Z., Zhang, J, and Wu, J., 2005b. 3D building modeling with digital map, lidar data and video image sequences. The Photogrammetric Record, 20(111), pp. 285-302.